

# 國立交通大學

電控工程研究所

博士論文

應用空域與時域腦動態分析於駕駛安全之雙重  
任務探討



Spatial and Temporal EEG-based Brain Dynamics  
of Dual-Task Driving Performance

研究生：陳世安

指導教授：林進燈 博士

中華民國 一 百 年 1 月

應用空域與時域腦動態分析於駕駛安全之雙重任務探討

Spatial and Temporal EEG-based Brain Dynamics of Dual-Task

Driving Performance Performance

研 究 生：陳世安

Student : Shi-An Chen

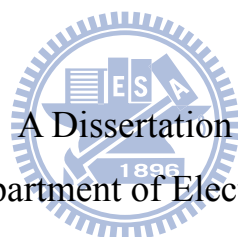
指導教授：林進燈 博士

Advisor : Dr. Chin-Teng Lin

國立交通大學

電控工程研究所

博士論文



Submitted to Department of Electrical Engineering

College of Electrical Engineering

National Chiao Tung University

in Partial Fulfillment of the Requirements

for the Degree of Doctor of Philosophy

in

Electrical Control Engineering

January 2011

Hsinchu, Taiwan, Republic of China

中華民國 一 百 年 1 月

# 應用空域與時域腦動態分析於 駕駛安全之雙重任務探討

學生：陳世安

指導教授：林進燈 博士

國立交通大學電控工程研究所

## 中文摘要

於行車中的駕駛者之分心發生已經被證實是造成車禍發生的重大原因之一。因此，本論文建立虛擬實境技術之動態駕車裝置，來模擬真實之駕車環境，透過分心場景的設計，結合腦電波(Electroencephalogram, EEG)分析來探討駕車行為下人類分心效應的腦部認知功能與反應變化。在此實驗中，我們建立雙重任務促使駕駛者造成分心效應，此雙重任務分別為非預期性的車子偏移與數學問題的出現。為了研究車子偏移與數學任務的交互作用與影響，我們建立了五個不同時間間隔(Stimulus Onset Asynchrony, SOA)的雙重任務實驗，並分析此雙重任務於不同五個時間間隔所反應出的行為表現與腦電波動態變化。腦電波訊號分析採用獨立成份分析演算法(Independent Component Analysis, ICA)來分離出不同獨立成份為獨立之訊號源，再將特定獨立訊號源套用事件相關頻譜擾動分析(Event Related Spectral Perturbation, ERSP)來觀察時域與頻域響應，藉此了解並比較不同時間上腦電波的頻譜差異。從我們的研究成果發現，額葉區(Frontal Lobe)之 Theta 頻帶與 Beta 頻帶的能量增強與駕駛者分心效應有正向關係，另外在運動皮質區(Motor Area)也觀察到 alpha 頻帶與 beta 頻帶能量抑制的發生，此上述成果是由

整合 15 位受測者的腦電波資料，也進行統計檢定分析。於行為表現上，我們觀察到不同時間間隔下反應時間的趨勢，與腦電波能量變化的趨勢是一致的，這說明了我們所發現的額葉區腦電波的能量增強現象，與行車中駕駛者分心效應發生有高度相關，而且能量增強越高，分心效應越強。

**關鍵字：**分心、認知、虛擬實境、不同時間間隔、獨立成份分析演算法、額葉區、theta 能量增強



# Spatial and Temporal EEG-based Brain Dynamics of Dual-Task Driving Performance

Student: Shi-An Chen

Advisor: Dr. Chin-Teng Lin

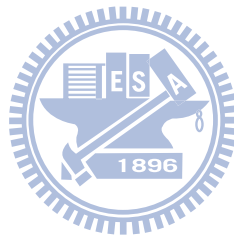
Institute of Electrical Control Engineering  
National Chiao Tung University

## Abstract

Driver distraction is a significant cause of traffic accidents. The aim of this study is to investigate Electroencephalography (EEG) dynamics in relation to distraction during driving. To study human cognition under a specific driving task, simulated real driving using virtual reality (VR) -based simulation and designed dual-task events are built, which include unexpected car deviations and mathematics questions. We designed five cases with different stimulus onset asynchrony (SOA) to investigate the distraction effects between the deviations and equations. The EEG channel signals are first converted into separated brain sources by independent component analysis (ICA). Then, event-related spectral perturbation (ERSP) changes of the EEG power spectrum are used to evaluate brain dynamics in time-frequency domains. Power increases in the theta and beta bands are observed in relation with distraction effects in the frontal cortex. In the motor area, alpha and beta power suppressions are also observed. All of the above results are consistently observed across 15 subjects. Additionally, further analysis demonstrates that response time and multiple cortical EEG power both

changed significantly with different SOA. This study suggests that theta power increases in the frontal area is related to driver distraction and represents the strength of distraction in real-life situations.

**Keyword:** distraction, cognition, virtual reality (VR), stimulus onset asynchrony (SOA), independent component analysis (ICA), frontal cortex, theta



## 致 謝

本論文的完成，首先要感謝指導教授林進燈博士這六年多來的悉心指導，讓我學習到許多寶貴的知識，在學業及研究方法上也受益良多。另外也要感謝口試委員們的建議與指教，使得本論文更為完整。

其次，感謝國立交通大學腦科學研究中心的柯立偉博士、邱添丁博士、同學黃騰毅、王俞凱、林弘章的相互砥礪，及所有學長、學弟們在研究過程中所給我的鼓勵與協助。尤其是柯立偉博士，在理論及程式技巧上給予我相當多的幫助與建議，讓我獲益良多。

感謝我的父母親對我的教育與栽培及物質上的一切支援，我的岳父岳母的提攜，感謝我的老婆雅婷在背後默默的支持我並給予我精神上的鼓勵，你的支持是我突破瓶頸與樂於接受新事物挑戰的原動力，並使我能安心地致力於學業，並順利完成論文。此外也感謝兩位姊姊對我不斷的關心與鼓勵。

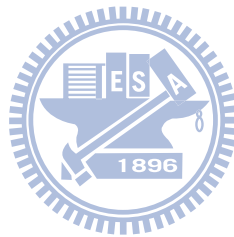
謹以本論文獻給我的家人及所有關心我的師長與朋友們。

# Contents

<b>Chinese Abstract .....</b>	<b>ii</b>
<b>English Abstract .....</b>	<b>iv</b>
<b>Chinese Acknowledgements .....</b>	<b>vi</b>
<b>Contents .....</b>	<b>vii</b>
<b>List of Tables.....</b>	<b>ix</b>
<b>List of Figures.....</b>	<b>x</b>
<b>1 Chapter 1 Introduction.....</b>	<b>1</b>
1.1 Motivation.....	1
1.2 Relevant Literatures .....	2
1.3 Dissertation Organization .....	4
<b>2 Chapter 2 Experimental Approach.....</b>	<b>5</b>
2.1 Dynamic Driving Environment.....	5
2.2 EEG Signal Acquisition .....	7
2.3 Experimental Design.....	8
2.3.1 Subject.....	8
2.3.2 VR Scenario .....	9
2.3.3 Task Descriptions.....	10
2.4 Data Analysis .....	11
2.4.1 Behavioral Performance.....	11
2.4.2 Distraction Effects of Dual-task.....	12
<b>3 Chapter 3 Experimental Results.....</b>	<b>18</b>
3.1 Behavioral Performance.....	18
3.2 Independent Component Clustering .....	19
3.3 Cluster Analysis .....	22
3.3.1 Frontal Cluster .....	22
3.3.2 Motor Cluster.....	25
3.3.3 Condition Comparison .....	28
<b>4 Chapter 4 Discussion .....</b>	<b>31</b>
4.1 Frontal Cluster .....	31
4.2 Motor Cluster.....	34

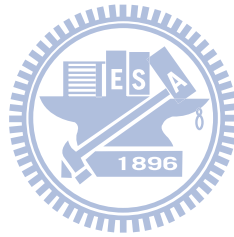


4.3 Other Clusters .....	35
4.4 More Behavioral Experiment.....	36
4.4.1 Subjects.....	36
4.4.2 Experiment Results .....	36
4.5 Dual-task Distraction Effects .....	40
4.6 Brain Dynamics Related to Behavioral Performance .....	43
<b>5 Chapter 5 CNN Implementation .....</b>	<b>46</b>
5.1 Cellular Neural Networks (CNN).....	46
5.2 CNN-based Hybrid-order Texture Segregation .....	46
5.2.1 Functions of Blocks .....	48
5.3 Experimental Results .....	52
5.4 Discussion.....	54
<b>6 Chapter 6 Conclusion .....</b>	<b>57</b>
<b>References.....</b>	<b>58</b>



# List of Tables

Table 3-1: The normalized response time to deviation and math .....	19
Table 3-2: The Number of Components in Different Clusters.....	22
Table 4-1: Summary data for responding car deviation and answering math equations variable across all trials (2187 trials for each condition), mean response time (Mean, in milliseconds), standard deviation (SD) and accuracy rate (AR).....	37



# List of Figures

Fig. 2-1: Pictures showed the dynamic VR driving environment, in the Brain Research Center of National Chiao Tung University, Taiwan, and ROC. A real car in the 3D VR environment was showed in the left picture. The experimental setup around the steering wheel was showed in the right picture.....5

Fig. 2-2: (a) The picture showed the configuration of the 3D surrounded scene. The 3D VR scene consisted of 7 projectors, creating a surrounded view. The frontal screen was overlapped by 2 projector frames in different polarizations, providing a stereoscopic VR scene for 3D visualization. (b) The 3D VR scene. .6

Fig. 2-3: Schematic pictures showed the lateral (A) and top view (B) of international 10-20 system of electrode placement.....7

Fig. 2-4: (a) The photomicrograph showed the simulated high way scene. The monotonous scene was designed to reduce the visual disturbance. (b) The illustration of the high way scene. The width of highway from the left to right side was equally divided into 256 units and the width of the car was 32 units. ...9

Fig. 2-5: The illustration shows the relationship of occurrences between the deviation and math tasks. D: deviation task onset, M: math task onset. (a) Case 1: math task presents 400ms before the deviation task onset. (b) Case 2: math and deviation tasks occur at the same time. (c) Case 3: math task presents 400ms after the deviation task onset. (d) Case 4: only math task presents. (e) Case 5: only deviation task occurs. The bottom insets show the onset sequences of the two tasks.....11

Fig. 2-6: The flow chart of EEG data analysis.....13

Fig. 2-7: How ICA work for source localization .....14

Fig. 2-8: ICA algorithm can separate 30 sources.....14

Fig. 2-9: The illustration of procedures in ERSP analysis. FFT was applied in each window with 256 samples, and there was 244-sample overlap of two adjacent windows. The time-dependent ERSP image was composed of the spectra of each window, and smoothed by 3-window moving average. In the final step, the significant parts of ERSP image were extracted by using bootstrap method. The pink dashed lines: the first event onset. The blue dashed lines: the averaged reaction time to the deviation. The red dashed lines: the averaged response time to math. The black dashed lines: averaged response time for the car returning to the third lane. Color bars showed the magnitude of ERSPs. ....15

Fig. 2-10: The flowchart of component clustering. Components from all subjects were classified into several significant clusters.....17

Fig. 3-1: This figure shows the bar charts of normalized response times. (a) for the math task and (b) for deviation task across 15 subjects. The filled black bar: case 1; dark gray bar: case 2; light gray bar: case 3; the open bar: single case. The response time for math task in dual-task cases (case 1, case 2, and case 3) is significantly longer than that for in single task (case 4). The shortest response time for the math onset is in case 4. The response time for deviation task in case 1 is significantly shorter than those in other cases. The longest response time to the deviation onset is in case 5. The bottom insets show the onset sequences of the two tasks.....18

Fig. 3-2: Baseline spectrum of the same components.....20

Fig. 3-3: The scalp maps and equivalent dipole source locations after IC clustering across 15 subjects. (a) the frontal components and (b) the left motor components are shown in the figure. There are 14 subjects in the frontal cluster and 11 subjects in the left motor cluster. The grand scalp map is the mean of the total component maps in each cluster. The smaller maps are the individual scalp maps. The right panels (c) and (d) show the 3-D dipole source locations (colored spheres) and their projections onto average brain images. The colored source locations correspond to their own scalp maps by the same color of the text above.....21

Fig. 3-4: The ERSP images of frontal cluster with five cases. (a) The ERSP images of frontal cluster with five cases. The right column show the onset sequences of the two tasks. Color bars indicate the magnitude of ERSPs. Red solid lines show the onset of the math task. Red dashed lines show the mean response time for the math task. Blue solid lines show the onset of the deviation task. Blue dashed lines show the mean response time for the deviation task. The red circle pointed out by the red arrow in case 2 means the red solid line and blue solid line are on the same position. Latencies calculated from (a) are shown in (b) by calculating time form the math task onset to the first occurrence of power increases. The open bars represent the latencies in the theta (4.5~9 Hz) band . The gray bars represent these latencies in the beta (11~15 Hz) band. The comparison of total power in cross-subject (14 subjects) averaged ERSP images in the frontal cluster between cases is shown in (c). The amount of total power is calculated by adding all the power increases in the same temporal period and the same frequency band. The open bars represent the total power in the theta band. The gray bars represent the total power in the beta band.....23

Fig. 3-5: Cross-subject ERSP plots for frequency (x-axis).....24

Fig. 3-6: Cross-subject ERSP plots for time interval (x-axis) .....24

Fig. 3-7: The ERSP images of the left motor cluster with five cases. (a) The ERSP images of the left motor cluster with five cases. The right column shows the onset sequences of the two tasks. Color bars indicate the magnitude of the ERSPs. Red solid lines show the onset of math. Red dashed lines show the mean response time for math task. Blue solid lines show the onset of deviation task. Blue dashed lines show the mean response time for deviation task. The red circle pointed out by a red arrow in case 2 means the red solid line and blue solid line are on the same position. Latencies calculated from (a) are shown in (b) by calculating from the deviation task onset to the first occurrence of power suppressions. The open bars represent the latencies in the alpha (8~14 Hz) band. The gray blue bars represent these latencies in the beta band (16~20 Hz). (c) shows the comparison of total power in cross-subject (11 subjects) averaged ERSP images in the left motor cluster between cases. The amount of total power is calculated by adding all the power suppressions in the same temporal period and the same frequency band. The open bars represent the total power in the alpha band. The gray bars represent the total power in the beta band. ....26

Fig. 3-8: Cross-subject ERSP plots for frequency (x-axis).....27

Fig. 3-9: Cross-subject ERSP plots for time interval (x-axis) .....27

Fig. 3-10: Compared ERSP.....28

Fig. 3-11: ERSP without a significance test and the differences between cases. Column (a) shows the ERSP in the frontal cluster without a significance test which contains all the details of case 1, case 2, case 3, and case 4. Column (b) shows the differences among three single-task cases in column (a). Column (c) shows the differences between single- and dual- task cases in column (a). Column (d) shows the ERSP in the left motor cluster without a significance test which contains all the details of case 1, case 2, case 3, and case 5. Column (e) shows the differences among three single-task cases in column (d). Column (f) shows the differences between single- and dual- task cases in column (d). A Wilcoxon signed-rank test ( $p < 0.01$ ) is used for the statistical test in (b), (c), (e), and (f).....29

Fig. 4-1: Picture showed the principle fissures and lobes cerebrum (Kandel et al.) The blue part is the frontal lobe and the white area is the location of parietal lobe. .32

Fig. 4-2: The trends of response time for the math task and EEG theta increases in the frontal cluster are consistent with one another.....33

Fig. 4-3: The scalp maps for the central midline (A), parietal (B), right motor (C), left occipital (D) and the right occipital (E) clusters across 15 subjects. Upper panels: the grand mean of the component map. Lower panels: individual scalp maps for the corresponded IC cluster.....35

Fig. 4-4: Statistical significance of the dual tasks in each condition was analyzed by repeated measures ANOVA followed by pair wise comparisons. Error bar indicates  $\pm 1 \cdot SE$ . Panel (a) shows mean response time for responding car deviation. The repeated measures ANOVA test reveals RT of  $-400ms$  SOA condition was significantly lower than those in other conditions. Panel (b) shows mean response time for answering math questions. The repeated measures ANOVA test results show that RT in the  $-400ms$  SOA condition was significantly higher than those in other conditions except in the  $0ms$  SOA condition. ....38

Fig. 4-5: Statistical significance of the dual tasks in each condition was analyzed by Friedman ANOVA followed by pair case comparisons using the Dunnett T3 method. Error bar indicates  $\pm 1 \cdot SE$ . Panel (a) shows normalized mean response score for responding car deviation. The Friedman ANOVA test reveals RT of  $-400ms$  SOA condition and single deviation task were significantly different. The test also reveals no significant differences existed among  $0ms$  SOA,  $400ms$  SOA and single deviation task conditions. Panel (b) shows the normalized mean response score for answering math equations. The Friedman ANOVA test results show that RT in the  $-400ms$  SOA condition was significantly higher than those in other conditions except in the  $0ms$  SOA condition. ....39

Fig. 4-6: An illustrative time diagram for the SOAs and a single task conditions. (a) In the  $-400ms$  SOA condition, overlap time of Task 1 and Task 2 is  $RT_1$  (high task overlap). (b) In the  $0ms$  SOA condition, overlap time of Task 1 and Task 2 is also  $RT_1$  (high task overlap). (c) In the  $400ms$  SOA condition, Task 1 and Task 2 overlap time is  $RT_1 - SOA$  (less than  $RT_1$ , low task overlap). (d) Only math equation presented. (e) Only deviation occurred. M: Math equation appeared; MR: Response math equations; D: Deviation appeared; DR: Response car deviation.....42

Fig. 5-1: The diagram of proposed algorithm.....47

Fig. 5-2: An example of Gabor filter dictionary. (a) represents the Gabor-type filter bank set, and (b) is the Feature space of Gabor filter dictionary. ....49

Fig. 5-3: The example of dividing of the input images.....52

Fig. 5-4: The simulation results of proposed algorithm.....53

Fig. 5-5: Histogram of error estimation .....55

# Chapter 1

## Introduction

### 1.1 Motivation

Driver distraction has been identified as the leading cause of car accidents. The U.S. National Highway Traffic Safety Administration had reported driver distraction as a high priority area about 20-30% of car accidents (Thomas, 2008). Distraction during driving by any cause is a significant contributor to road traffic accidents (Horberry et al., 2006; Patten et al., 2004). Driving is a complex task in which several skills and abilities are simultaneously involved. Distractions found during driving are quite widespread, including eating, drinking, talking with passengers, using cell phones, reading, feeling fatigue, solving problems, and using in-car equipment. Commercial vehicle operators with complex in-car technologies also cause an increased risk as they may become increasingly distracting in the years to come (Dukic et al., 2006; Lee et al., 2001). Some literature studied the behavioral effect of driver's distraction in car. Tijerina et al. (2000) showed driver distraction from measurements of the static completion time of an in-vehicle task. Similarly, distraction effects caused by talking on cellular phones during driving have been a focal point of recent in-car studies (Hancock et al., 2003; Strayer et al., 2003; Hahn et al., 2000). Experimental studies have been conducted to assess the impact of specific types of driver distraction on driving performance. Though these studies generally reported significant driving impairment (Crundall et al., 2006; Amado and Ulupinar, 2005), simulator studies cannot provide information about accidents due to impairment resulting in hospitalization of the driver. To provide information before the occurrence of crashes, the drivers' physiological responses are investigated in this dissertation. However, monitoring drivers' attention-related brain resources is still a challenge for

researchers and practitioners in the field of cognitive brain research and human–machine interaction.

## 1.2 Relevant Literatures

Regarding neural physiological investigation, some literature focused on the brain activities of “divided attention,” referring to attention divided between two or more sources of information, such as visual, auditory, shape, and color stimuli. Positron emission tomography (PET) measurements were taken while subjects discriminated among shape, color, and speed of a visual stimulus under conditions of selective and divided attention. The divided attention condition activated the anterior cingulate and prefrontal cortex in the right hemisphere (Corbetta et al., 1991). In another study, functional magnetic resonance imaging (fMRI) was used to investigate brain activity during a dual-task (visual stimulus) experiment. Findings revealed activation in the posterior dorsolateral prefrontal cortex (middle frontal gyrus) and lateral parietal cortex (Koechlin et al., 1999). In addition, several neuroimaging studies showed the importance of the prefrontal network in dual-task management (Szameitat et al., 2006; Stelzel et al., 2005). Some studies investigated traffic scenarios recorded the EEG to compare P300 amplitudes (Baldwin and Coyne, 2003). During simulated traffic scenarios, resource allocation was assessed as an event-related potential (ERP) novelty oddball paradigm (Rakauskas et al., 2005). In these EEG studies, however, only the time course was analyzed. Deiber et al. (2007) took one more step to analyze the relation between time and frequency courses. Their study used EEG to investigate mental arithmetic-induced workload and found theta band power increases in areas of the frontal cortex. Despite so much research on brain activities, the above-mentioned studies only investigated brain activities during dual-task interactions without considering the SOA problem during driving, which is with the temporal gap between presentations of two stimuli. When dual tasks are presented within a short SOA,



the response time of each task is typically lower than that presented within a longer SOA (Levy and Pashler, 2001). Therefore, the current study investigates the effects of the different temporal relationships of stimuli.

Clinical practices as well as basic scientific studies have been using the EEG for 80 years. Presently, EEG measurement is widely used as a standard procedure in research such as sleep studies (Lin et al., 2005b; Lin et al., 2008), epileptic abnormalities, and other disorder diagnoses. Compared to another widely used neuroimaging modality, fMRI, the EEG is much less expensive and has superior temporal resolution in investigating SOA problems. To avoid interference and decrease risks while operating a vehicle on the road, researchers adopted driving simulations for vehicle design. Studies of driver's behavior and cognitive states are also expanding rapidly (Eoh et al., 2005). However, static driving simulation cannot fully create real-life driving conditions, such as the vibrations experienced when driving an actual vehicle on the road. Therefore, the VR-based simulation with a motion platform was developed (Lin et al., 2005a; Kemeny and Panerai, 2003). This VR technique allows subjects to interact directly with a virtual environment rather than only monotonic auditory or visual stimuli. Integrating realistic VR scenes with visual stimuli makes it easy to study the brain response to attention during driving. Therefore, in recent years, VR-based simulation combined with EEG monitoring is a recent and beneficial innovation in cognitive engineering research.

The main goal of this study is to investigate the brain dynamics related to distraction by using EEG and a VR-based realistic driving environment. Unlike previous studies, the experiment design has three main characteristics. First, the SOA experimental design, with different appearance times of two tasks, has the benefit of investigating the driver's behavioral and physiological response under multiple conditions and multiple distraction levels. Second,

ICA-based advanced analysis methods are used to extract brain responses and the cortical location related to distraction. Third, this study investigates the interaction and effects of dual-task-related brain activities, in contrast to a single task.

## **1.3 Dissertation Organization**

The dissertation was organized in 6 chapters. Chapter 1 briefly introduced current state in the drivers' distraction and the goal of the study. Chapter 2 detailed the experimental approach and materials of the study. Chapter 2 also described the details of experimental setup, including different conditions under the time course of event onset asynchrony setup. In chapter 3, we explored the EEG with innovative methods by combining Independent Component Analysis (ICA), time-frequency spectral analysis, and component clustering. The behavioral performance analysis was also shown in Chapter 3. Chapter 4 showed discussions about what the EEG results mean and the correlation between physiological and behavioral data. Chapter 5 described a possible implementation of EEG application by using CNN features and architectures. Finally we concluded in Chapter 6.

# Chapter 2

## Experimental Approach

### 2.1 Dynamic Driving Environment

A virtual-reality (VR) based highway-driving environment was used to investigate the changes on drivers' distraction effect. The VR driving environment includes 3D surround scenes projected by seven projectors and a real car mounted on a 6-degree-of-freedom (as showed in Fig. 2-1) Stewart platform to provide the kinesthetic stimuli. The dynamic driving environment provided a safe, time saving and low cost approach to study human cognition under realistic driving events. The subjects could interact directly with the environment and receive the most realistic driving conditions during the experiments.



Fig. 2-1: Pictures showed the dynamic VR driving environment, in the Brain Research Center of National Chiao Tung University, Taiwan, and ROC. A real car in the 3D VR environment was showed in the left picture. The experimental setup around the steering wheel was showed in the right picture.

The VR scene was generated by the Virtual- Reality technology with a World Tool Kit

(WTK) library. The C program including the WTK library was used and its library function was called up to move the three-dimensional models. The 3D view was composed of seven identical PCs running the same VR program. Seven PCs were synchronized by LAN so all scenes were going at exactly same pace. The VR scenes of different viewpoints were projected on corresponding locations. Fig. 2-2(a) showed the layout of our simulator. The front screen marked 1 and 2 was overlapped by two polarized frames to reach the binocular parallax. The frames for the left and right eyes were projected onto the frontal screen with two projectors, respectively. By wearing special glasses with a polarized filter, the configuration provided a stereoscopic VR scene for a 3D visualization. In our VR scene, the surrounded screens covered  $206^\circ$  frontal FOV and  $40^\circ$  back FOV, as shown in Fig. 2-2(b). Frames projected from 7 projectors were connected side by side to construct a surrounded VR scene. The size of each screen had diagonal measuring 2.6-3.75 meters. The vehicle was placed at the center of the surrounded screens.

a



b



Fig. 2-2: (a) The picture showed the configuration of the 3D surrounded scene. The 3D

VR scene consisted of 7 projectors, creating a surrounded view. The frontal screen was overlapped by 2 projector frames in different polarizations, providing a stereoscopic VR scene for 3D visualization. (b) The 3D VR scene.

## 2.2 EEG Signal Acquisition

An electrode cap was mounted on the subject's head for signal acquisition as shown in Fig. 2-5. A standard for the placement of EEG electrodes proposed by Jasper in 1958, which is known as the 10-20 International System of Electrode Placement (URL: <http://faculty.washington.edu/chudler/1020.html>) is used in the electrode cap. An illustration of the 10-20 system is shown in Fig. 2-5, the electrodes are named according to the location of an electrode and the underlying area of cerebral cortex.

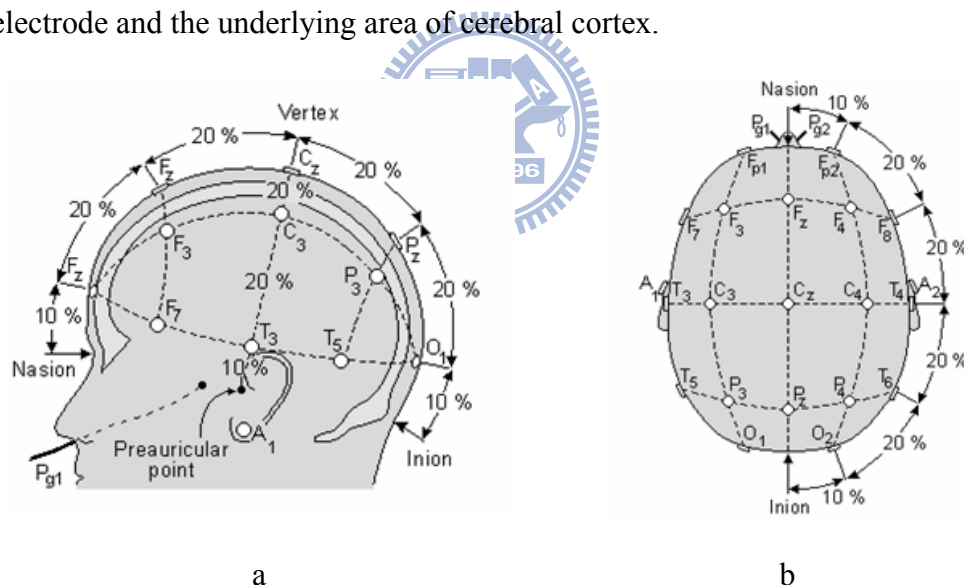


Fig. 2-3: Schematic pictures showed the lateral (A) and top view (B) of international 10-20 system of electrode placement

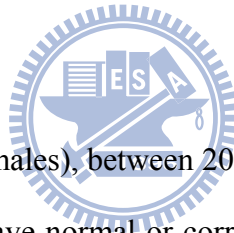
The letters F, C, T, P, and O were refer to the frontal, central, temporal, parietal, and occipital cortical regions on the scalp, respectively. The term “10-20” means 10% and 20% of the total distance between specified skull locations. The percentage-based system allowed

differences in skull locations. The physiological data acquisition used 30 sintered Ag/AgCl EEG/EOG electrodes with a unipolar reference at right earlobe and 2 ECG channels in bipolar connection placed on the chest.

Thirty scalp electrodes (Ag/AgCl electrodes with a unipolar reference at the right earlobe) by the NuAmp system (Compumedics Ltd., VIC, Australia) were mounted on the subject's head to record the physiological EEG (Lin et al., 2010). The EEG electrodes were placed based on a modified international 10-20 system. The contact impedance between EEG electrodes and the cortex was calibrated to be less than 10 k $\Omega$ .

## 2.3 Experimental Design

### 2.3.1 Subject



Fifteen healthy subjects (all males), between 20 and 28 years of age, were recruited from the university population. They have normal or corrected-to-normal vision, are right handed, have a driver's license, and are reported being free from psychiatric or neurological disorders. Written informed consent was obtained prior to the study.

Each subject participated in four simulated sessions inside a car with hands on the steering wheel to keep the car in the center of the third lane, which was numbered from the left lane, in a VR surround scene on a four-lane freeway (Lin et al., 2005a). Before beginning first session, each subject took a 15~30 minute for practice session. In each session, subjects proceeded to a freeway simulated driving lasting fifteen minutes with the corresponding EEG signals synchronously recorded. For these four-session experiments, subjects were required to rest for ten minutes between every two sessions to avoid fatigue.

### 2.3.2 VR Scenario

We developed a VR highway environment with a monotonic scene as shown in Fig. 2-4(a) and eliminated all unnecessary visual stimuli. The four lanes from left to right were separated by a median strip in the VR-based scene. The distance from the left side to the right side of the road was equally divided into 256 points for outputting digital signal from WTK program, and the width of each lane and the car was 60 units and 30 units, respectively (as showed in Fig. 2-4(b)). In the VR scene, the simulated driving speed was controlled by a scheduled program, thus subjects need not to step on paddles, to prevent large muscle activity on the throttle or brake.

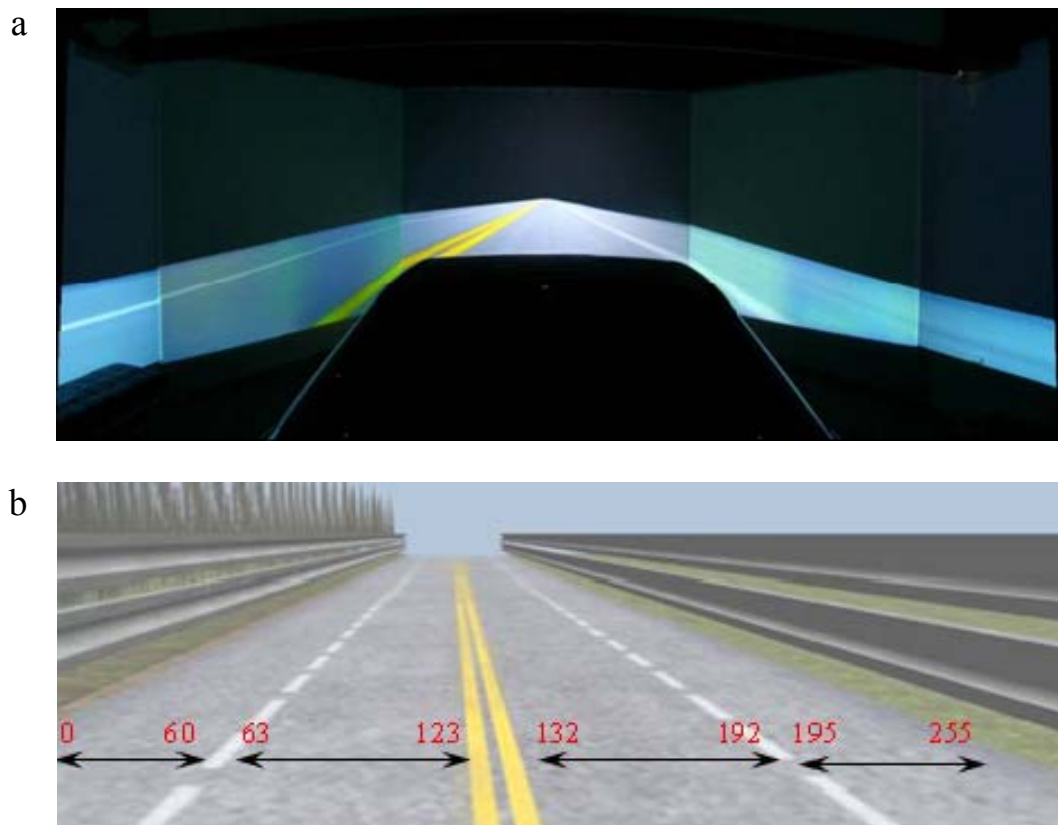


Fig. 2-4: (a) The photomicrograph showed the simulated high way scene. The monotonous scene was designed to reduce the visual disturbance. (b) The illustration of the high way scene. The width of highway from the left to right side was equally

divided into 256 units and the width of the car was 32 units.

### **2.3.3 Task Descriptions**

Since the main purpose of this dissertation is to investigate distraction effects in dual-task conditions, two tasks involving unexpected car deviations and mathematical questions were designed. In the driving task, the car frequently and randomly drifted from the center of the third lane. Subjects were required to steer the car back to the center of the third lane. This task mimicked the effects of driving on a non-ideal road surface. In the mathematical task, two-digit addition equations were presented to the subjects. The answers were designed to be either valid or invalid. Subjects were asked to press the right or left button on the steering wheel corresponding to on correct or incorrect equations, respectively. The allotment ratio of correct-incorrect equations was 50-50. The choice of mathematic task was motivated by the desire for control in the task demands (Geary and Wiley, 1991). All drivers could perform this mathematic task well without training.

To investigate the effects of SOA between two tasks, the combinations of these two tasks were designed to provide different distracting conditions to the subjects as shown in Fig. 2-5. Five cases were developed to study the interaction of the two tasks. The bottom insets show the onset sequences of two tasks. Therefore, this study investigated the relationship of math task and driving task and how two tasks affected each other in the SOA conditions.



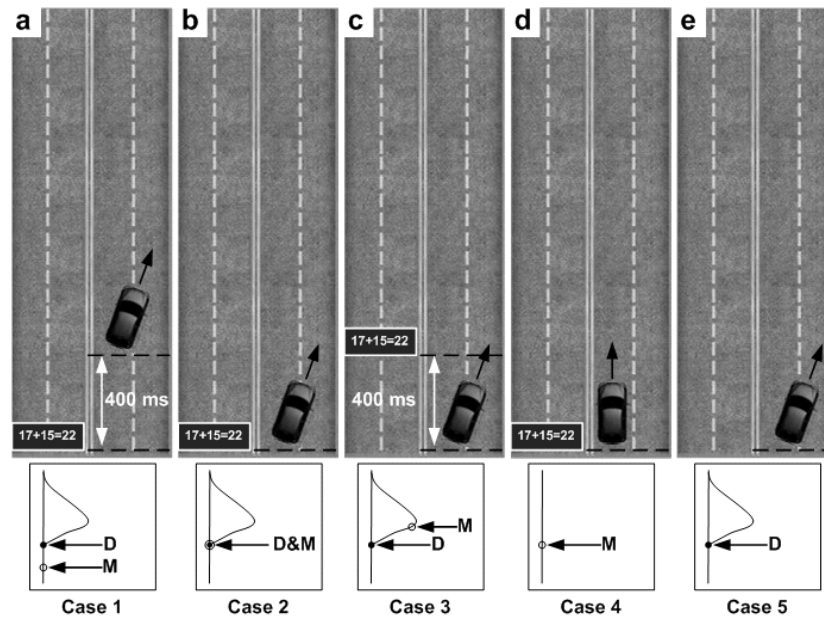


Fig. 2-5: The illustration shows the relationship of occurrences between the deviation and math tasks. D: deviation task onset. M: math task onset. (a) Case 1: math task presents 400ms before the deviation task onset. (b) Case 2: math and deviation tasks occur at the same time. (c) Case 3: math task presents 400ms after the deviation task onset. (d) Case 4: only math task presents. (e) Case 5: only deviation task occurs. The bottom insets show the onset sequences of the two tasks.

## 2.4 Data Analysis

### 2.4.1 Behavioral Performance

After recording the behavioral data, statistical package for the social science (SPSS) Version 13.0 for Windows software is applied to estimate the significance testing of behavioral data. The response time of these two tasks (the driving deviation and the math equation) is analyzed to study the behavior of subjects in the experiments.

Using ANOVA (analysis of variance), the significances of the response time of these two tasks are tested for every subject. A non-parametric test is also utilized to study the trends of

the behavioral data. Firstly, this study excluded outliers, comprising around 6.57 % of all trials, based on the criteria that response time was distributed outside the mean response time plus three times the standard deviation of each single session. Secondly, the number of trials in one of five cases which is minimal is chosen to make a benchmark to randomly select the same number of trials in other cases. Thirdly, a single task is taken for the baseline to normalize the behavioral data to be  $\frac{X_i}{X_{\text{mean}}}$  ( $X_i$ : mean of response time in case  $i$ ,  $X_{\text{mean}}$ : mean of response time in single case). For example, in order to compare the distraction effects from the math equation, case 4 (the single math task) is the baseline.

## 2.4.2 Distraction Effects of Dual-task

EEG epochs are extracted from the recorded EEG signals with 16-bit quantization, at the sampling rate of 500Hz. The data are then preprocessed using a simple low pass filter with a cut-off frequency of 50 Hz to remove line noise and other high frequency noise. One more high-pass filter with a cut-off frequency of 0.5 Hz is utilized to remove DC drift. This study adopts ICA to separate independent brain sources (Jung et al., 2000; Lee et al., 1999; Makeig et al., 1995). ERSP technology is then applied to these independent component (IC) signals (separated independent brain sources) to transfer the signal into the time-frequency domain for the event-related frequency study. Finally, the stability of component activations and scalp topographies of meaningful components are investigated with component clustering technology. Because different cases with various combinations of driving and the math tasks are designed, EEG responses from five different cases are extracted separately.

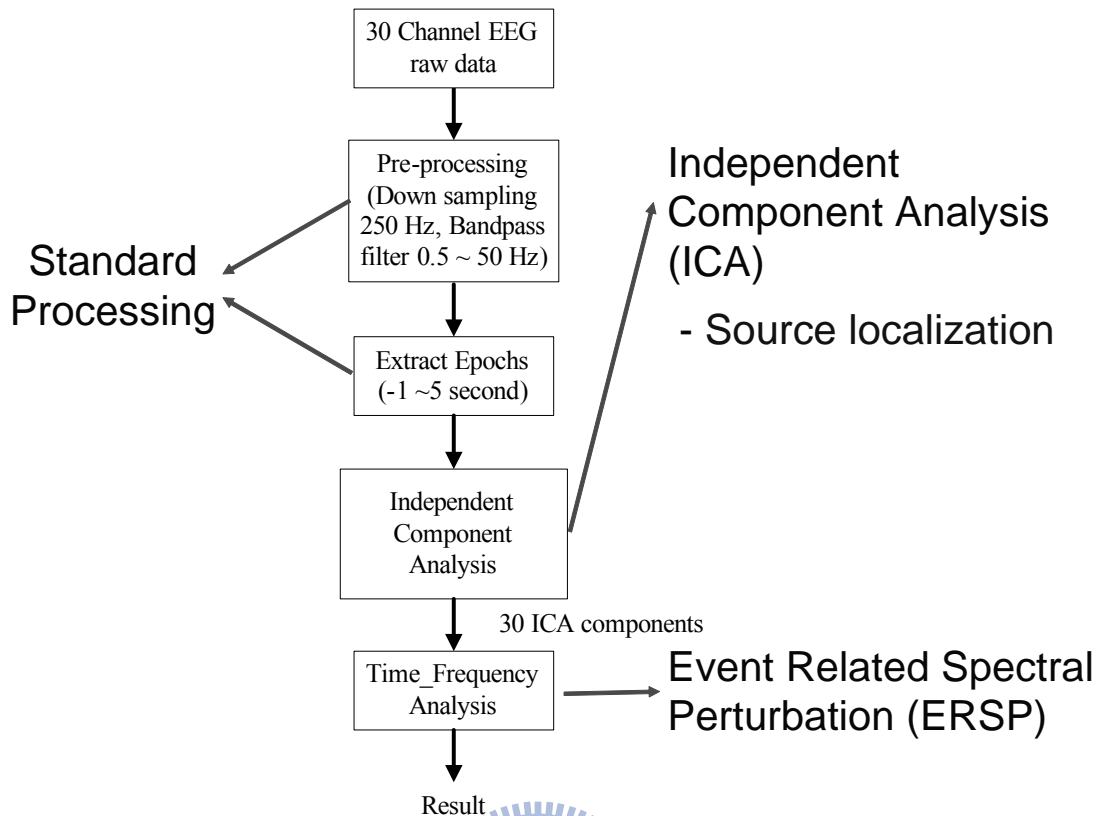


Fig. 2-6: The flow chart of EEG data analysis

EEG source segregation, identification, and localization are very difficult because EEG data collected from the human scalp induce brain activities within a large brain area. Although the conductivity between the skull and brain is different, the spatial “smearing” of EEG data caused by volume conduction does not cause a significant time delay. This suggests that ICA algorithm is suitable for performing blind source separation on EEG data. The first applications of ICA to biomedical time series analysis were presented by Makeig and Inlow (1993). Their report shows segregation of eye movements from brain EEG phenomena, and separates EEG data into constituent components defined by spatial stability and temporal independence. Subsequent technical experiments demonstrated that ICA could also be used to remove artifacts from both continuous and event-related (single-trial) EEG data (Jung et al., 2000; Lee et al., 1999). Presumably, multi-channel EEG recordings are mixtures of underlying brain sources and artificial signals. By assuming that (a) mixing medium is linear

and propagation delays are negligible, (b) the time courses of the sources are independent, and (c) the number of sources is the same as the number of sensors; that is, if there are N sensors, the ICA algorithm can separate N sources (Jung et al., 2000).

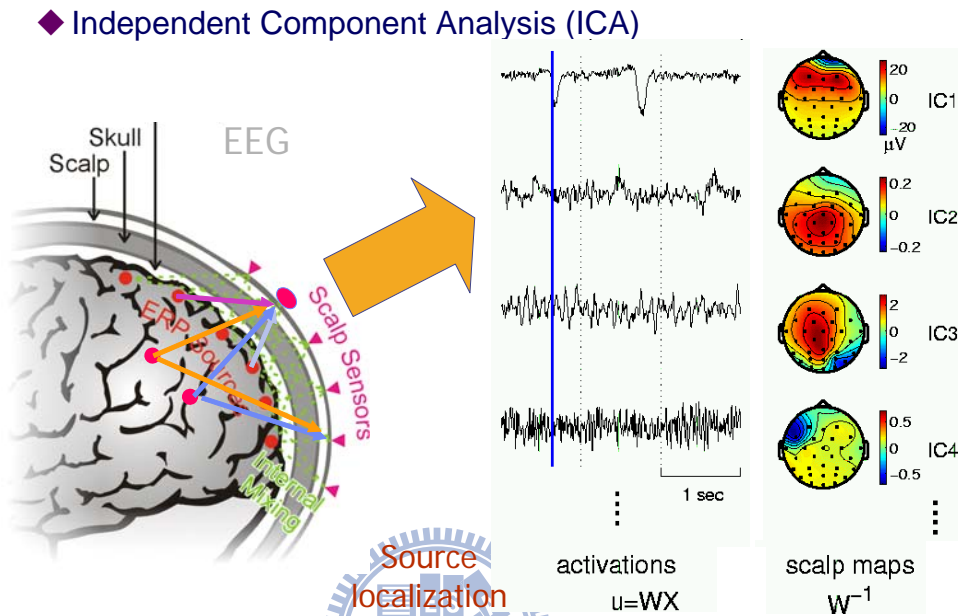


Fig. 2-7: How ICA work for source localization

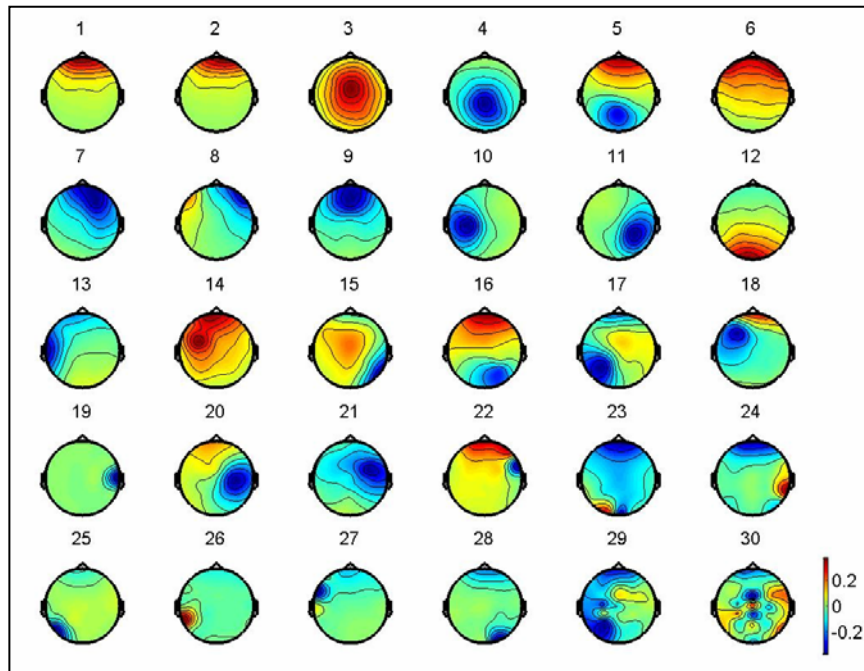


Fig. 2-8: ICA algorithm can separate 30 sources

The time sequences of ICA component signals are subjected to Fast Fourier Transform with overlapped moving windows (in Fig. 2-9). In addition, the spectrum in each epoch is smoothed by 3-window (768 points) moving-average to reduce random errors. The spectrum prior to event onsets is considered as the baseline spectrum for every epoch. The mean of the baseline spectrum is subtracted from the power spectral after stimulus onsets so spectral “perturbation” can be visualized. This procedure is then applied repeatedly to every epoch. The results are averaged to yield ERSP images (Makeig, 1993). These measures can evaluate averaged dynamic changes in amplitudes of the broad band EEG spectrum as a function of time following cognitive events. The ERSP images mainly show spectral differences after an event since the baseline spectrum prior to event onsets had been removed. After performing a bootstrap analysis (usually 0.01 or 0.03 or 0.05; here 0.01 was applied) on ERSP, only statistically significant ( $p < 0.01$ ) spectral changes are shown in the ERSP images. Non-significant time/frequency points are masked (replaced with zero). Consequently, any perturbations in the frequency domain become relatively prominent.

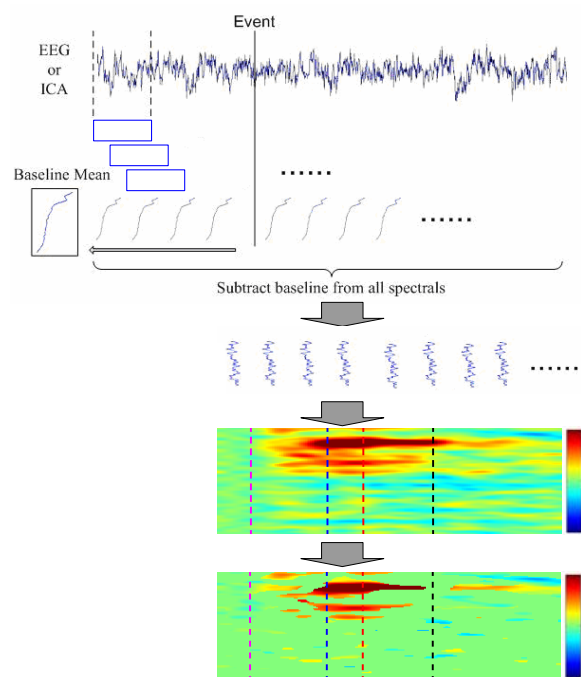


Fig. 2-9: The illustration of procedures in ERSP analysis. FFT was applied in each

window with 256 samples, and there was 244-sample overlap of two adjacent windows. The time-dependent ERSP image was composed of the spectra of each window, and smoothed by 3-window moving average. In the final step, the significant parts of ERSP image were extracted by using bootstrap method. The pink dashed lines: the first event onset. The blue dashed lines: the averaged reaction time to the deviation. The red dashed lines: the averaged response time to math. The black dashed lines: averaged response time for the car returning to the third lane. Color bars showed the magnitude of ERSPs.

To study the cross-subject component stability of ICA decomposition, components from multiple subjects are clustered, based on their spatial distributions and EEG characteristics. However, components from different subjects differ in many ways such as scalp maps, power spectrum, ERPs and ERSPs. Some studies attempted to solve this problem by calculating similarities among different ICs (Makeig et al., 2002; Makeig et al., 2004; Onton et al., 2005). Based on these studies, ICs of interest are selected and clustered semi-automatically based on their scalp maps, dipole source locations, and within-subject consistency (in Fig. 2-10). To match scalp maps of ICs within and across subjects in this dissertation, the gradients of the IC scalp maps from different sessions of the same subject are computed and grouped together based on the highest correlations of gradients of the common electrodes retained in all sessions. For dipole source locations, DIPFIT2 routines from EEGLAB are used to fit single dipole source models to the remaining IC scalp topographies using a four-shell spherical head model (Oostenveld and Oostendorp, 2002). In the DIPFIT software, the spherical head model is co-registered with an average brain model (Montreal Neurological Institute) and returns approximate Talairach coordinates for each equivalent dipole source.

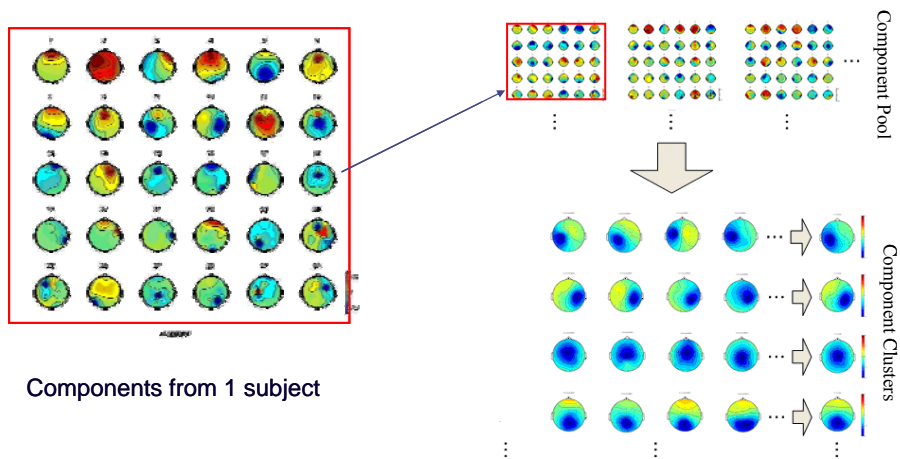


Fig. 2-10: The flowchart of component clustering. Components from all subjects were classified into several significant clusters.



# Chapter 3

## Experimental Results

### 3.1 Behavioral Performance

To investigate the overall behavioral index, this study uses nonparametric tests because several extremely large scores are significantly skewed. Firstly, the trials of data are randomly selected to have the same number of the trials in all cases. Then, the response time of the deviation and math tasks in the five cases are normalized to correspond to single-deviation and single-math cases, respectively. SPSS software is used for the Friedman test, and the results of which are shown in Fig. 3-1. Dual-task cases are marked for easy discrimination from single-task cases.

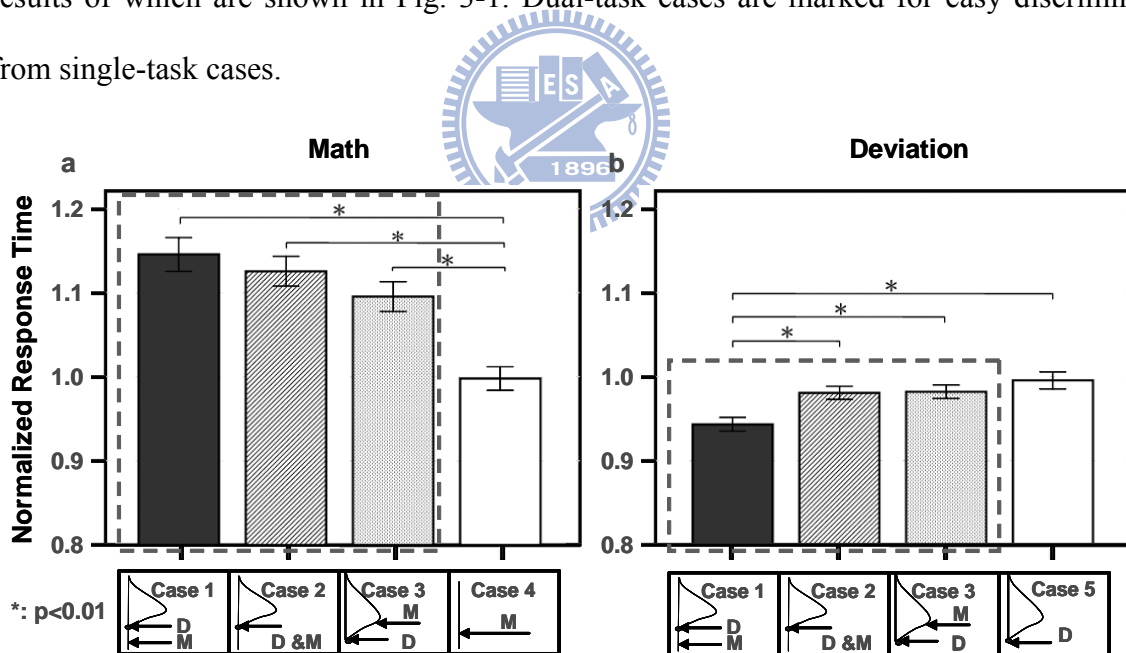


Fig. 3-1: This figure shows the bar charts of normalized response times. (a) for the math task and (b) for deviation task across 15 subjects. The filled black bar: case 1; dark gray bar: case 2; light gray bar: case 3; the open bar: single case. The response time for math task in dual-task cases (case 1, case 2, and case 3) is significantly longer than that for in single task (case 4). The shortest response time for the math



onset is in case 4. The response time for deviation task in case 1 is significantly shorter than those in other cases. The longest response time to the deviation onset is in case 5. The bottom insets show the onset sequences of the two tasks.

To know how the cases make the differences, the Student-Newman-Keuls test is used for the post hoc test (in Table 3-1). The test statistic on response time of math tasks in cases 1-4, is  $\chi^2(3)=903.926$  from the Friedman's ANOVA test, and  $p<0.01$ . The Student-Newman-Keuls test show three significant groups: case 1 with case 2, case 3, and case 4 in which the response time for math task in case 1 is the longest. Statistical test results of the response time for deviation tasks in cases 1-3, and case 5, is  $\chi^2(3)=493.98$  from the Friedman's ANOVA test, and  $p<0.01$ . Using the Student-Newman-Keuls test, there are two significant groups: case 1, and the other cases in which the response time for deviation task in case 1 is the shortest.

Table 3-1: The normalized response time to deviation and math

Case	Response time to deviation			Response time to math		
	Mean	Standard deviation	Difference (dual-single)	Mean	Standard deviation	Difference (dual-single)
Case 1	0.9480	0.1314	$p<0.01$	1.1479	0.3061	$p<0.01$
Case 2	0.9856	0.1269	$p>0.01$	1.1277	0.2724	$p<0.01$
Case 3	0.9865	0.1231	$p>0.01$	1.0975	0.2727	$p<0.01$
Single (baseline)	1	0.1553		1	0.2168	

### 3.2 Independent Component Clustering

EEG epochs are extracted from the recorded EEG signals. Then, ICA is utilized to

decompose independent brain sources from the EEG epochs. Based on distraction effects in this study, many brain resources are involved in this experiment. Especially, the motor component is active when subjects are steering the car. At the same time, activations related to attention in the frontal component appear. Therefore, ICA components, including frontal and motor, are selected for IC clustering to analyze cross-subject data based on their EEG characteristics, such as baseline spectrum, Scalp map and Dipole plot.

Based on the baseline spectrum of their EEG characteristics, the baseline spectrums of the same components of different subjects are listed in the Fig. 3-2. The outlier can be observed and removed. In this case (frontal component), green subject is the outlier.

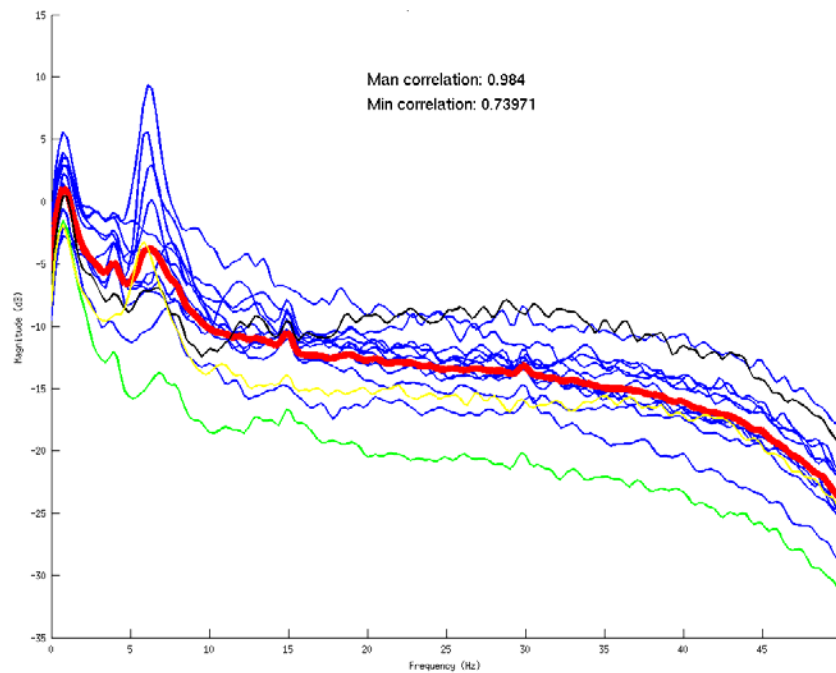


Fig. 3-2: Baseline spectrum of the same components

Then, IC clustering groups massive components from multiple sessions and subjects into several significant clusters. Cluster analysis, k-means, is applied to the normalized scalp topographies and power spectra of all 450 (30 channels x 15 subjects) components from the 15 subjects. Cluster analysis identifies at least 7 component clusters having similar power spectra and scalp projections. These 7 distinct component clusters consisted of frontal, central

midline, parietal, left/right motor and left/right occipital. Table 3-2 gives the number of components in different clusters. This investigation uses the frontal and left motor components to analyze distraction effects. Fig. 3-3 shows the scalp maps and equivalent dipole source locations for frontal and left motor clusters. Based on this finding, the EEG sources of different subjects in the same cluster are from the same physiological component.

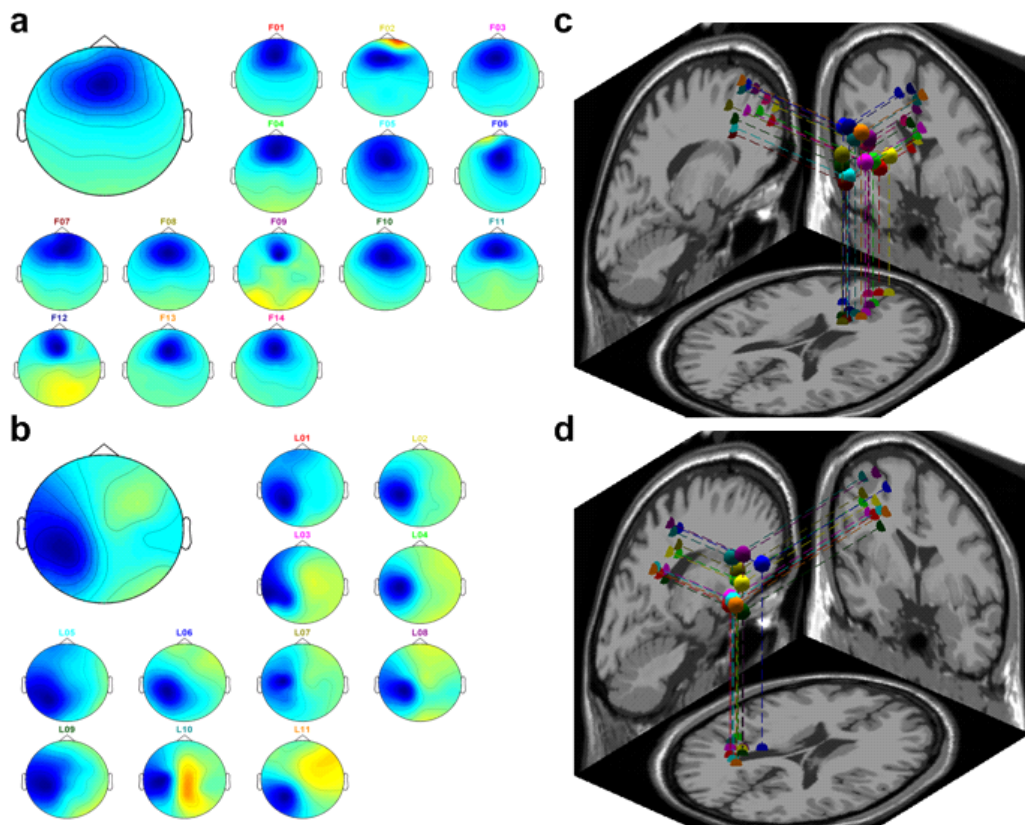


Fig. 3-3: The scalp maps and equivalent dipole source locations after IC clustering across 15 subjects. (a) the frontal components and (b) the left motor components are shown in the figure. There are 14 subjects in the frontal cluster and 11 subjects in the left motor cluster. The grand scalp map is the mean of the total component maps in each cluster. The smaller maps are the individual scalp maps. The right panels (c) and (d) show the 3-D dipole source locations (colored spheres) and their projections onto average brain images. The colored source locations correspond to their own scalp maps by the same color of the text above.

Table 3-2: The Number of Components in Different Clusters

	Frontal	Central Midline	Parietal	Left Motor	Right Motor	Left Occipital	Right Occipital
Number of components	14	7	6	11	6	7	5

### 3.3 Cluster Analysis

#### 3.3.1 Frontal Cluster

Fig. 3-4a shows the cross-subject averaged ERSP in the frontal cluster corresponding to the five cases. This figure also reveals significant ( $p < 0.01$ ) power increases related to the math task, demonstrating that the power increases in the frontal cluster are related to the math task. The theta power increases in three dual-task cases including cases 1-3 are slightly different from each other. Compared to the single math task (case 4), the power in dual-task cases is stronger. Especially, the power increase in case 1 is the strongest. On the beta band, it also shows power increases, which appear only in the math-task and time-locked to mathematics onsets.

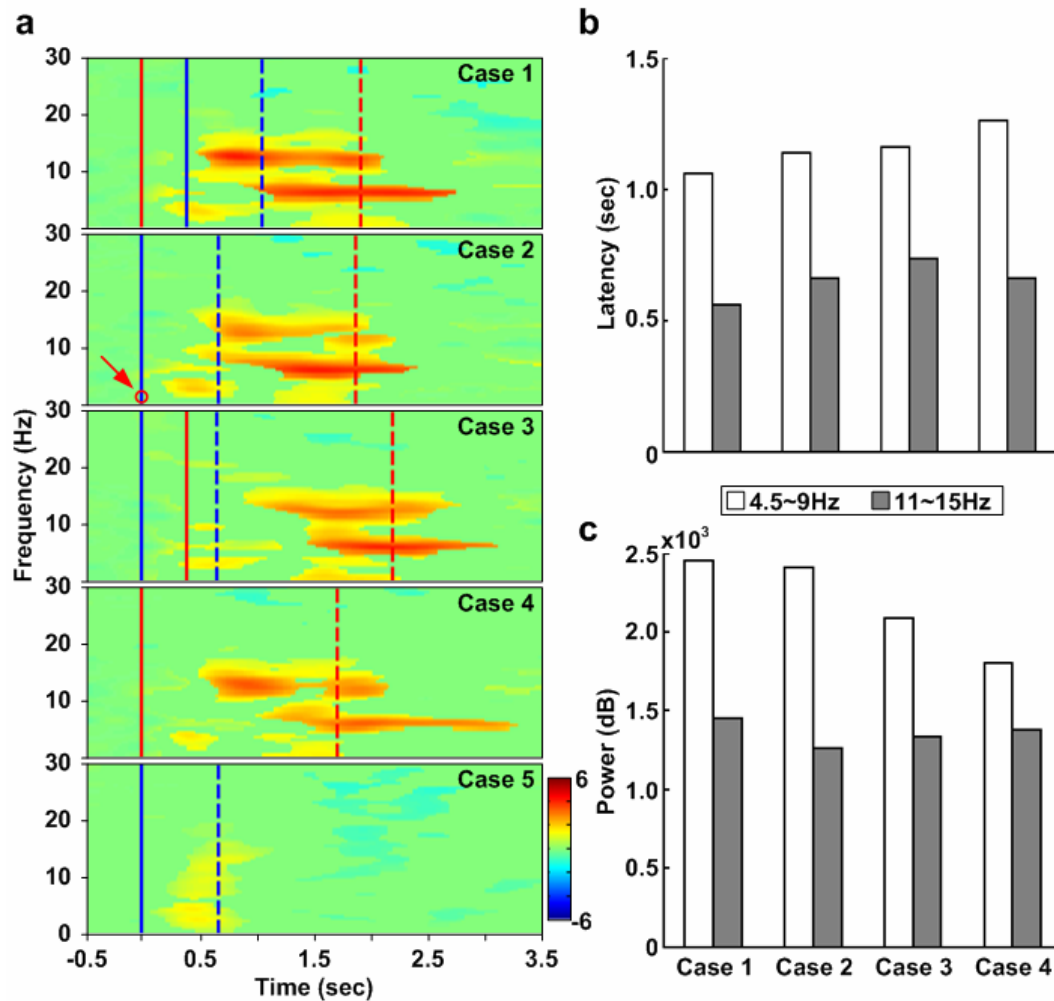


Fig. 3-4: The ERSP images of frontal cluster with five cases. (a) The ERSP images of frontal cluster with five cases. The right column show the onset sequences of the two tasks. Color bars indicate the magnitude of ERSPs. Red solid lines show the onset of the math task. Red dashed lines show the mean response time for the math task. Blue solid lines show the onset of the deviation task. Blue dashed lines show the mean response time for the deviation task. The red circle pointed out by the red arrow in case 2 means the red solid line and blue solid line are on the same position. Latencies calculated from (a) are shown in (b) by calculating time from the math task onset to the first occurrence of power increases. The open bars represent the latencies in the theta (4.5~9 Hz) band. The gray bars represent these latencies in the beta (11~15 Hz) band. The comparison of total power in cross-subject (14 subjects) averaged ERSP images in the frontal cluster between cases is shown in (c). The amount of total power

is calculated by adding all the power increases in the same temporal period and the same frequency band. The open bars represent the total power in the theta band. The gray bars represent the total power in the beta band.

In order to find out the suitable and reasonable range of EEG power in Fig. 3-4a, the ranges of frequency are firstly calculated in Fig. 3-5. Then the ranges of the frequency band are defined as “theta band: 4.5 ~ 9Hz” and “beta band: 11 ~ 15Hz”. After defining the ranges of frequency, the ranges of time interval are calculated in Fig. 3-6. Then the ranges of time interval are defined as “theta band: 300~3500 ms” and “beta band: 500~2600 ms”.

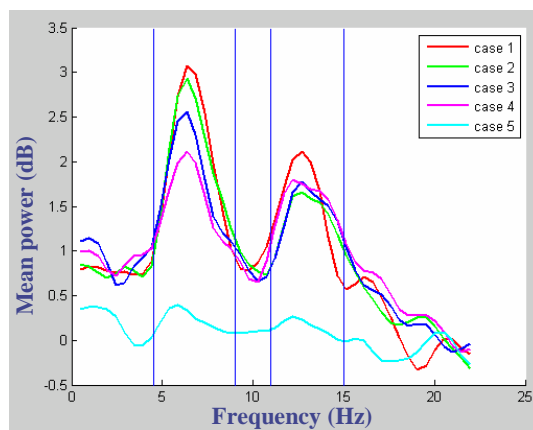


Fig. 3-5: Cross-subject ERSP plots for frequency (x-axis)

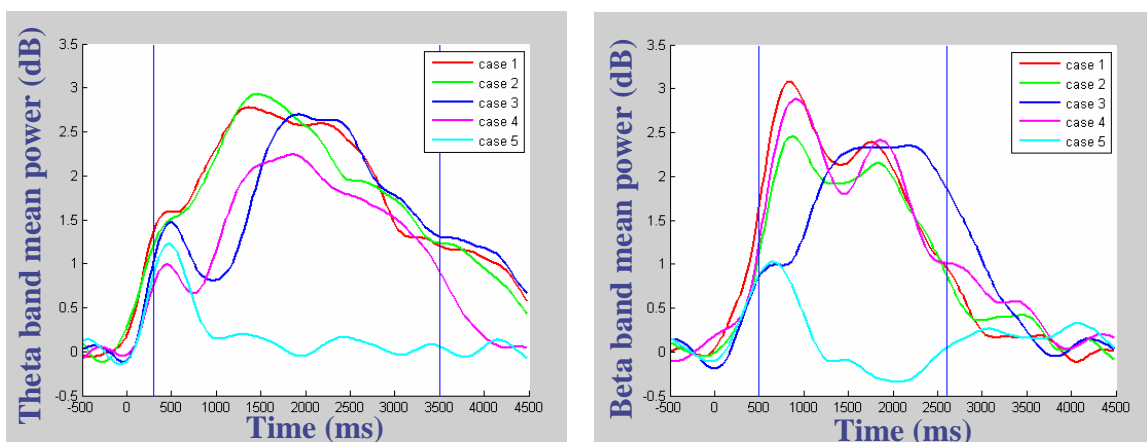


Fig. 3-6: Cross-subject ERSP plots for time interval (x-axis)

Fig. 3-4b and c give comparisons of the latency and total power in four cases from Fig. 3-4a. It demonstrates that the latencies of power increases in two frequency bands are different with the different SOA time. The shortest latencies in both bands occur in case 1 and the longest power increase latency in the theta band occurs in case 4. It also demonstrates that the amount of power increases in the theta band is different with the different SOA time. The most significant power increase occurs in case 1.

### **3.3.2 Motor Cluster**

Fig. 3-7a shows the cross-subject average ERSP in the left motor cluster corresponding to five cases. Significant ( $p < 0.01$ ) power suppressions appear around the event onsets (at 0ms) and stop at different time axes by cases. In case 4, the alpha and beta power suppressions appear continuously until the red dashed lines, which indicates the mean of the response time for the math task. Compared with case 4, the alpha and beta power suppressions in case 5 are stronger and also last longer. In other cases, the alpha and beta power suppressions continue after the blue dashed lines. This phenomenon is suggested to be related to steering the car back to the center of the third lane.

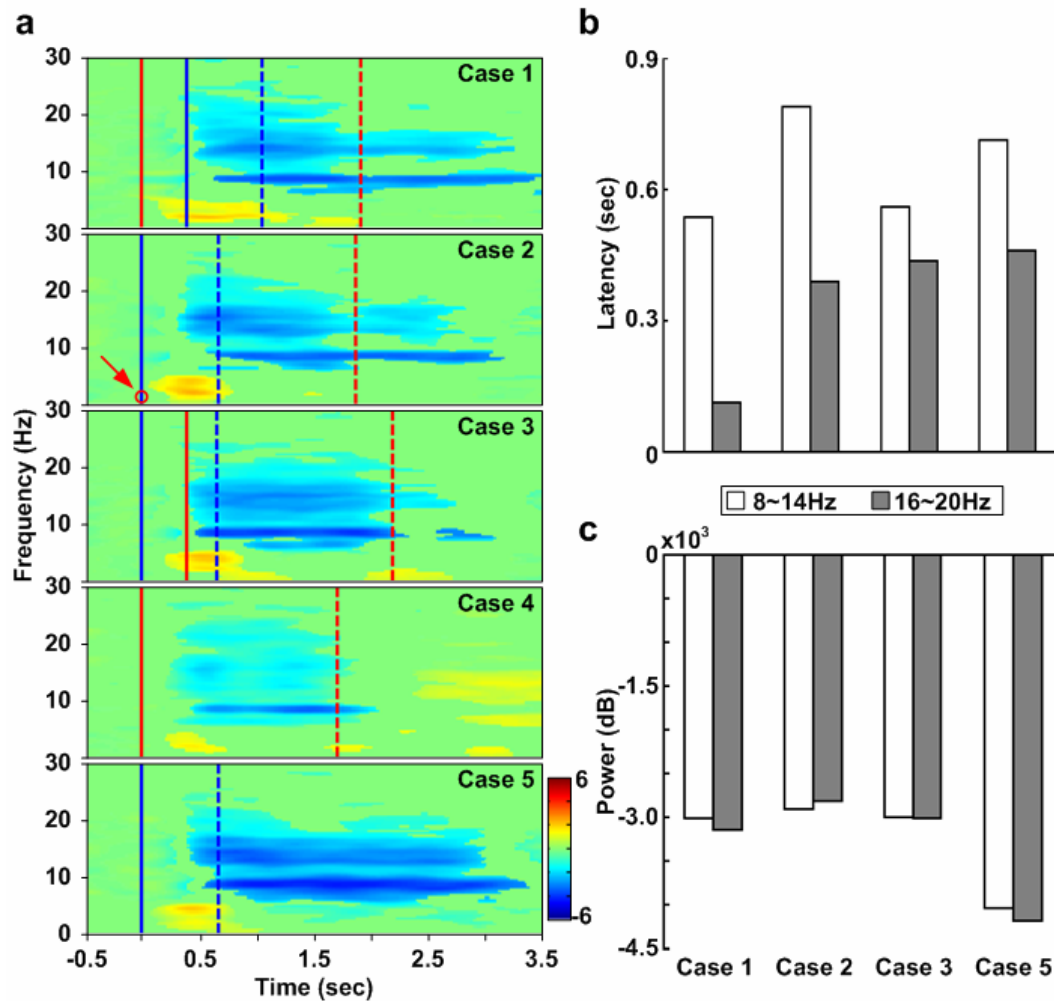


Fig. 3-7: The ERSP images of the left motor cluster with five cases. (a) The ERSP images of the left motor cluster with five cases. The right column shows the onset sequences of the two tasks. Color bars indicate the magnitude of the ERSPs. Red solid lines show the onset of math. Red dashed lines show the mean response time for math task. Blue solid lines show the onset of deviation task. Blue dashed lines show the mean response time for deviation task. The red circle pointed out by a red arrow in case 2 means the red solid line and blue solid line are on the same position. Latencies calculated from (a) are shown in (b) by calculating from the deviation task onset to the first occurrence of power suppressions. The open bars represent the latencies in the alpha (8~14 Hz) band. The gray blue bars represent these latencies in the beta band (16~20 Hz). (c) shows the comparison of total power in cross-subject (11 subjects) averaged ERSP images in the left motor cluster between cases. The



amount of total power is calculated by adding all the power suppressions in the same temporal period and the same frequency band. The open bars represent the total power in the alpha band. The gray bars represent the total power in the beta band.

In order to find out the suitable and reasonable range of EEG power in Fig. 3-7a, the ranges of frequency are firstly calculated in Fig. 3-8. Then the ranges of the frequency band are defined as “mu suppression: 8 ~ 14Hz” and “beta band: 16 ~ 20Hz”. After defining the ranges of frequency, the ranges of time interval are calculated in Fig. 3-9. Then the ranges of time interval are defined as “mu suppression: 400~3700 ms” and “beta band: 200~3400 ms”.

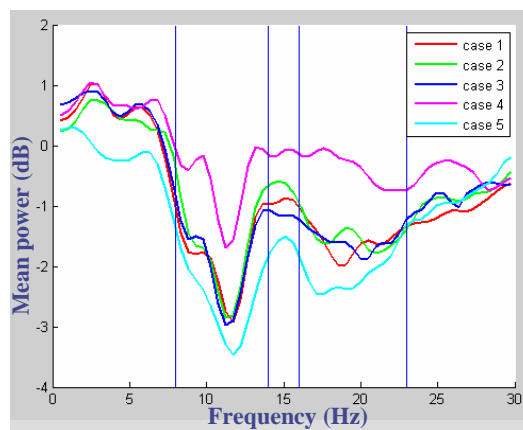


Fig. 3-8: Cross-subject ERSP plots for frequency (x-axis)

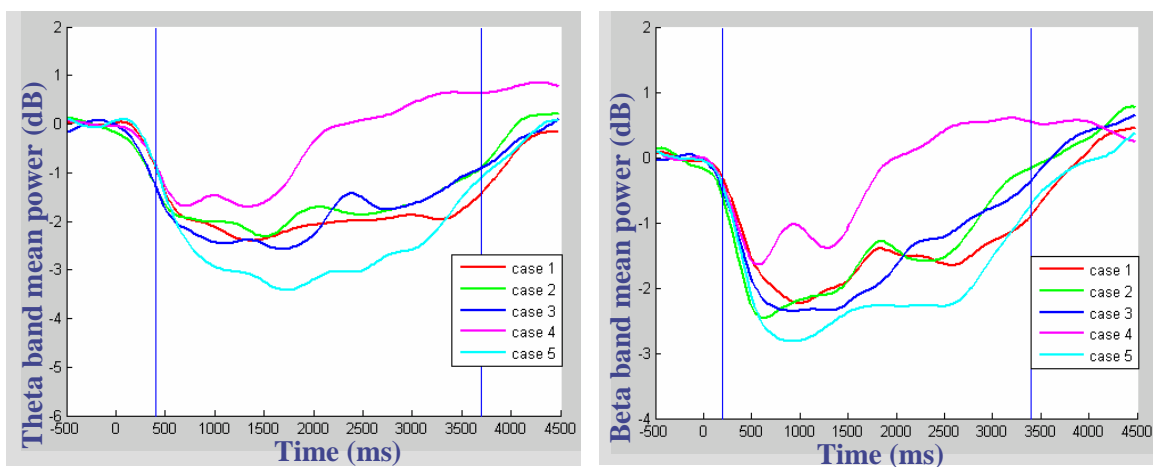


Fig. 3-9: Cross-subject ERSP plots for time interval (x-axis)

Fig. 3-7b and c shows comparisons of the latency and total power between the four cases in Fig. 3-7a. It demonstrates that power suppression latencies in the beta band are different with the different SOA time. The shortest power suppression latency occurs in case 1 and the longest power increase latency occurs in case 5. It also demonstrates that the amount of power suppression in the alpha band is different with the different SOA time. The most significant power suppression occurs in case 5 (the single driving task) and the smallest power suppression occurs in case 4 (the single math task).

### 3.3.3 Condition Comparison

In order to compare two ERSP in different case, we apply a compared ERSP method with a statistic test in Fig. 3-10. The results will have some black circles with the original ERSP. The areas inside the black circles mean the area with significant power.

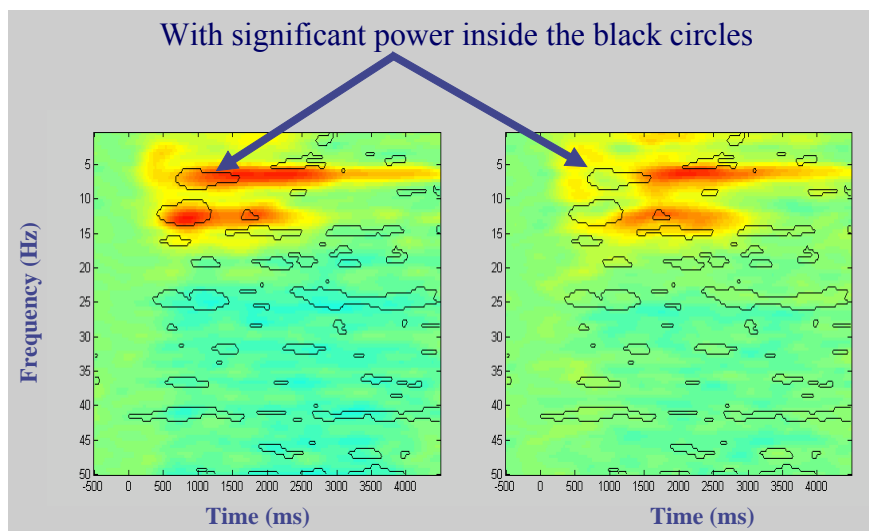


Fig. 3-10: Compared ERSP

Fig. 3-11a and d show the ERSP in the frontal and left motor clusters without a

significance test. Columns (b) and (e) show the differences among three single-task cases; columns (c) and (f) show the differences between single- and dual- task cases. In columns (b), (c), (e), and (f), a Wilcoxon signed-rank test is used to retain the regions with significant power inside the black circles. Columns (b) and (c) show the comparison of power increases between cases. The remained regions show greater power increases in the single-task case than in the dual-task case. Columns (e) and (f) show compared power suppressions between cases. The remained regions show greater power suppressions in the dual-task cases than in the single-task case.

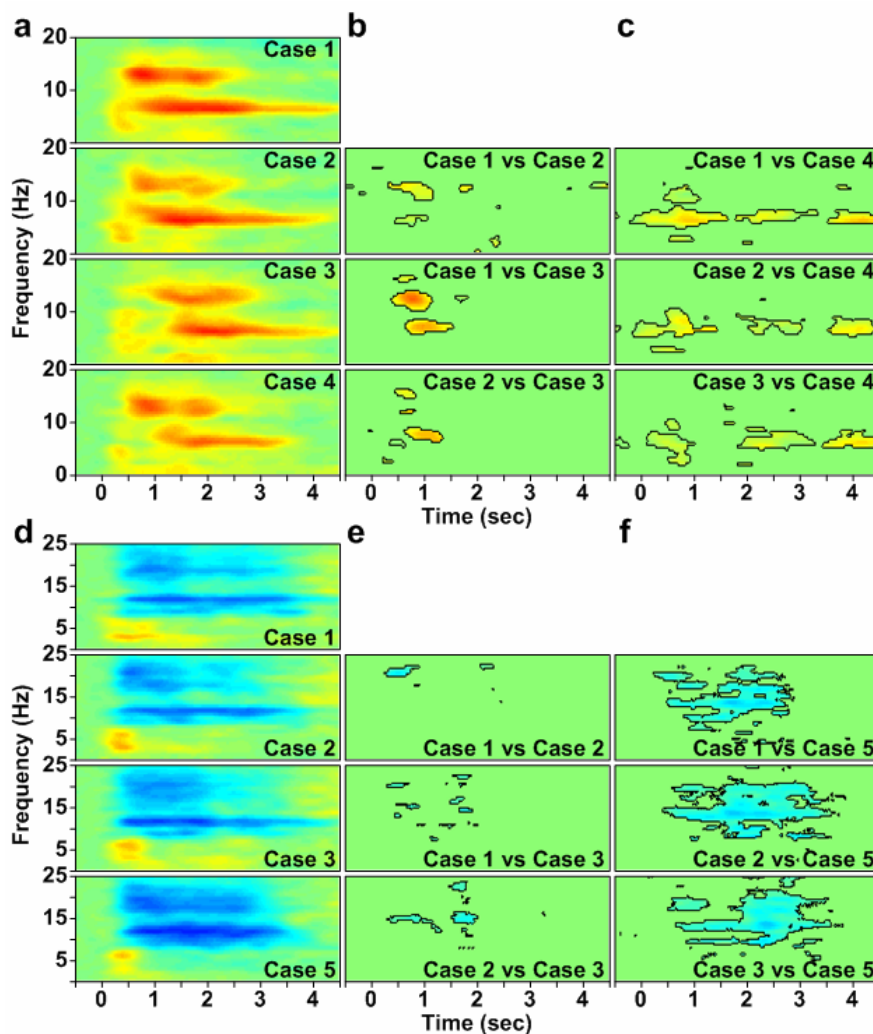
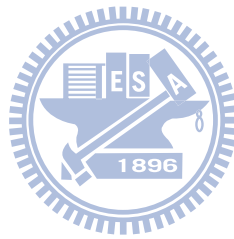


Fig. 3-11: ERSP without a significance test and the differences between cases.

Column (a) shows the ERSP in the frontal cluster without a significance test which

contains all the details of case 1, case 2, case 3, and case 4. Column (b) shows the differences among three single-task cases in column (a). Column (c) shows the differences between single- and dual- task cases in column (a). Column (d) shows the ERSP in the left motor cluster without a significance test which contains all the details of case 1, case 2, case 3, and case 5. Column (e) shows the differences among three single-task cases in column (d). Column (f) shows the differences between single- and dual- task cases in column (d). A Wilcoxon signed-rank test ( $p < 0.01$ ) is used for the statistical test in (b), (c), (e), and (f).



# Chapter 4

## Discussion

The brain dynamics related to distracted effects of stimulus onset asynchrony (SOA) by using EEG and VR-based realistic driving environment was investigated. The SOA experimental design was to investigate the distracted level. In this Chapter, the results after cross-subject analysis would be discussed. Cross-subject analysis was able to prove that the appeared features were not restricted to specific subject or experiment, that was, it could ensure the stability and consistency of pour findings.

### 4.1 Frontal Cluster

The frontal lobe is an area in the brain, located at the front of each cerebral hemisphere (in Fig. 4-1). The frontal area deals with impulse control, judgment, language production, working memory, motor function, and problem solving (Burgess, 2000; Sarnthein et al., 1998). In Fig. 3-4a, the greater frontal power increases in cases 1-4 appear due to the solving of the math questions. The power increases in the theta (4.5~9 Hz) and beta bands (11~15Hz) appear briefly after the math onset. Fig. 3-4b and c show the quantified frontal power latencies and power increases in four conditions for the purpose of discussing the EEG dynamics made by solving the math question. In the theta power, the shortest latency is revealed in case 1. Power increases in three dual-task cases are higher than that in single-task case with the greatest power occurring in case 1. These phenomena suggest that dual tasks induce more event-related theta activities as well as subjects need more brain resources to accomplish dual tasks. The theta increase is associated with numerous processes such as mental work load, problem solving, encoding, or self monitoring (Onton et al., 2005). Based on this evidence, the study demonstrates that the subjects were distracted under dual-task conditions in the

experiment.

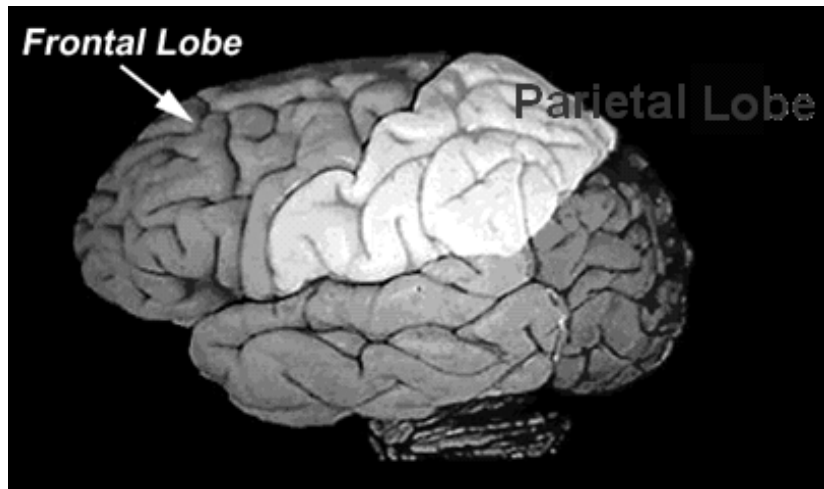


Fig. 4-1: Picture showed the principle fissures and lobes cerebrum (Kandel et al.) The blue part is the frontal lobe and the white area is the location of parietal lobe.

Since human visual sensors need about 300 ms to induce event-related potential (P300 activity, Jensen et al., 2001), we have also tested several kind of intervals between first and second task, 400 ms between two tasks is sufficient for a subject to perceive stimulus. In case 1, a processing task is already in the brain and subjects need more brain resources to manage the high priority task presented 400 ms after the processing task. Therefore, the total power in the theta band in case 1 is the highest as shown in Fig. 3-4c. Clearly the theta power increase appears the earliest in case 1 as shown in Fig. 3-4b. The early theta response in the frontal area primarily reflects the activation of neural networks involved in allocating attention related to the target stimulus (Missonnier et al., 2006).

The trends of response time for the math task (in Fig. 3-1a) and EEG theta increases in the frontal cluster (in Fig. 3-4c) are consistent with one another (in Fig. 4-2). In the case of the single math task, the response time is the shortest and the theta power increase is the weakest. Among the dual-task cases, the longest response time and the greatest theta power increase

are in case 1. This evidence suggests that the theta activity of the EEG in the frontal area during dual tasks is related to distraction effects and represents the strength of distraction. In addition, power increases in the beta band appear in all cases. From the ERSP images, the patterns are time-locked to the onset of the math task. Fernández et al. (1995) suggested that significant EEG beta band differences in the frontal area are due to a specific component of mental calculation.

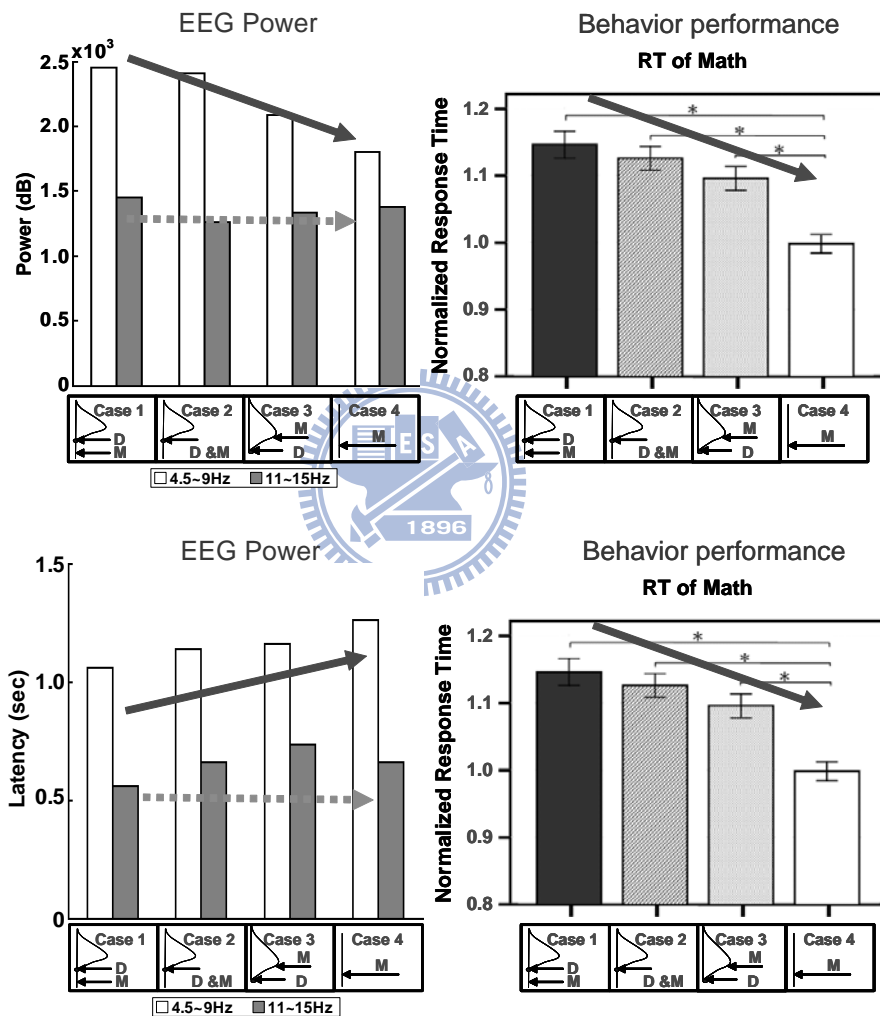


Fig. 4-2: The trends of response time for the math task and EEG theta increases in the frontal cluster are consistent with one another.

## 4.2 Motor Cluster

Mu rhythm ( $\mu$  rhythm) is an EEG rhythm usually recorded from the motor cortex of the dominant hemisphere. It can be suppressed by simple motor activities such as clenching the fist of the contra lateral side, or passively moved (Kuhlman, 1978a; Kuhlman, 1978b; Schoppenhorst et al., 1980). Mu suppression is believed to be the electrical output of the synchronization on large portions of pyramidal neurons in the motor cortex that controls hand and arm movements.

In this study, the mu suppressions (8~14 Hz) and beta power suppression (16~20Hz) are mostly caused by subjects steering the wheel and pressing buttons as shown in Fig. 3-7a. The mu suppressions caused by steering the wheel are almost time-locked to the response onset of driving task in cases 1-3 and case 5. However, the mu suppressions caused by pressing the buttons have no effects in case 4. As for in the dual-task cases, the mu suppressions are weaker than those in single-task case. This may due to the competition of brain resources required by wheel steering and button pressing.

Thus, Fig. 3-7b and Fig. 3-7c show motor power latencies and power increases in 4 cases for the purposes of discussing the EEG dynamics caused by the driving task. In (b), the longest latency of beta power suppression is observed in case 5 and the shortest latency appears in case 1. Perhaps motor planning is involved in preparing for steering the wheel and answering the math questions (Hayhoe et al., 2003). In (c), the three dual-task power suppressions are weaker than those in single task. Based on above evidences, it suggests that math processing occupies more brain resources in the frontal area during dual-task cases so less activation is induced in the motor area.



## 4.3 Other Clusters

To study the cross-subject component stability of ICA decomposition, components from multiple sessions and subjects were clustered based on their spatial distributions and EEG characteristics. Component clustering grouped massive components from multiple sessions and subjects into several significant clusters. Cluster analysis, k-means, applied to the normalized scalp topographies and power spectra of all 450 (30 channels x 15 subjects) components from the 15 subjects, and identified at least 7 clusters of components having similar power spectra and scalp projections.

These component clusters also showed functionally distinct activity patterns. Five other distinct component clusters (as shown in Fig. 4-3) accounted for central midline, parietal, right motor and left/right occipital, respectively. These were effectively removed from the activity of the other component clusters by the ICA decomposition and are not further considered here. The numbers of components in different clusters were given in Table 3-2.

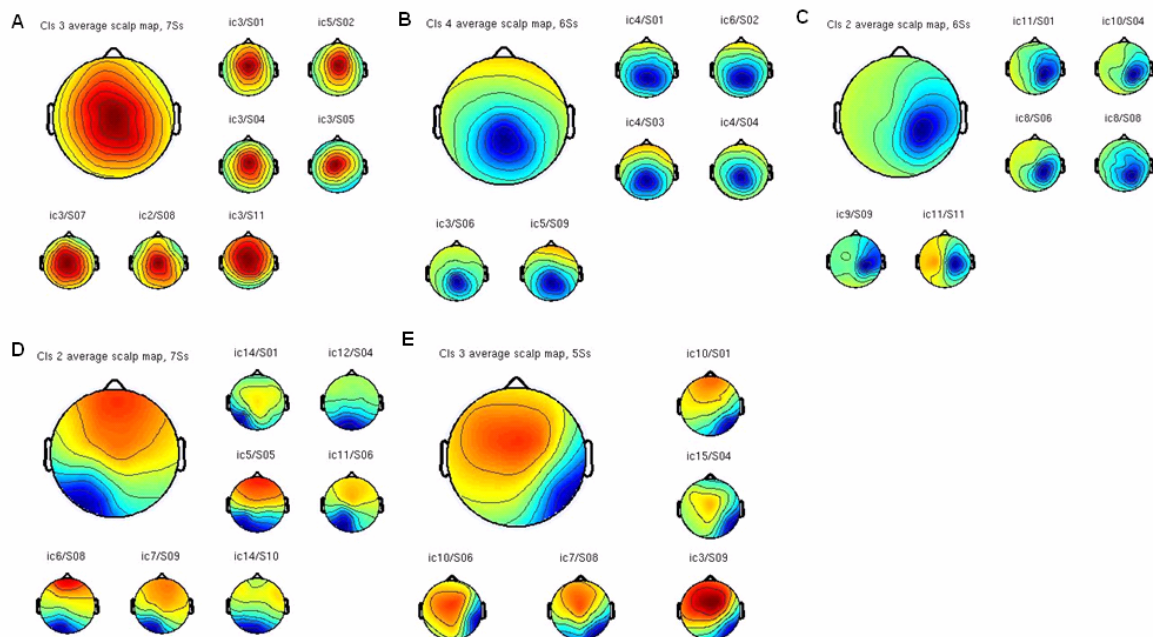


Fig. 4-3: The scalp maps for the central midline (A), parietal (B), right motor (C), left

occipital (D) and the right occipital (E) clusters across 15 subjects. Upper panels: the grand mean of the component map. Lower panels: individual scalp maps for the corresponded IC cluster.

## **4.4 More Behavioral Experiment**

In order to have more powerful result, the number of subject should be more. Due to the original number is 15 and the behavioral results don't have enough significant difference, we invited more subjects to participate this experiment with only behavioral response recorded.

### **4.4.1 Subjects**

The total number of volunteer subjects was 25 in this study. The mean age of subjects was 26.2 years, and the standard deviation of age was 2.9 years. All subjects owned a valid driving license and had a mean reported driving experience of 5 years. All subjects were free of neurological and psychological disorders, as well as drug and alcohol abuse. Experimental procedures were approved by the Institutional Review Board of Taipei Veterans General Hospital.

### **4.4.2 Experiment Results**

The mean and the standard deviation of RT in the four different conditions were listed in Table 4-1. In responding the car deviation task, the mean RT of single-task condition was the longest (656.2 ms). In answering the math equation task, the mean RT of single-task condition was 1700.9 ms and was clearly shorter than other conditions. In comparison with RTs of responding the car deviation and answering the

math equation in single-task conditions, subjects used more resources and took more time on answering the math equation which showed that answering the math equation task could be as a distracting factor because its difficulty was harder than responding the car deviation task.

Table 4-1: Summary data for responding car deviation and answering math equations variable across all trials (2187 trials for each condition), mean response time (Mean, in milliseconds), standard deviation (SD) and accuracy rate (AR).

Types	Mean	SD	AR (%)
<b>Responding the car deviation</b>			
<b>Dual-task condition</b>			
-400 ms SOA (math first and then deviation onset)	627.9	108.0	—
0 ms SOA (math and deviation occurred simultaneously)	650.5	115.3	—
400 ms SOA (deviation onset first then math)	648.0	114.1	—
<b>Single-task condition</b>			
Only car deviation	656.2	130.5	—
<b>Answering the math equation</b>			
<b>Dual-task condition</b>			
-400 ms SOA (math first and then deviation onset)	1972.2	673.9	94.6
0 ms SOA (math and deviation occurred simultaneously)	1943.5	633.4	94.1
400 ms SOA (deviation onset first then math)	1852.4	592.0	93.9
<b>Single-task condition</b>			
Only the math equation	1700.9	468.5	94.6

Fig. 4-4a and Fig. 4-4b show the bar chart of the mean and the standard deviation of RT in responding the car deviation task and answering the math equation task, respectively. In responding the car deviation task, the mean RT under the -400ms SOA condition (mean RT equals 627.9ms) was significantly shorter than the other three conditions (mean RT range was

from 648.0 to 656.2 ms) according to the repeated measures ANOVA ( $F_{3,2186} = 75.64, p < 0.01$ ) statistics test. Specifically, the mean RT in the single-task condition was longer than that in dual-task conditions. In answering the math equation task, the mean RT in the  $-400\text{ms}$  SOA condition (mean RT =  $1972.2\text{ms}$ ) were longer than the other three conditions (mean RT range,  $1943.5$  to  $1700.9\text{ms}$ ) according to the repeated measures ANOVA ( $F_{3,2186} = 257.63, p < 0.01$ ) statistics test. Specifically, the mean RT in the single-task condition was significantly shorter than that in dual-task conditions.

In addition, overall accuracy of answering math equations was over 94%. There were no significant effects within three dual-task conditions ( $\chi^2(3) = 1.837, p > 0.01$ ).

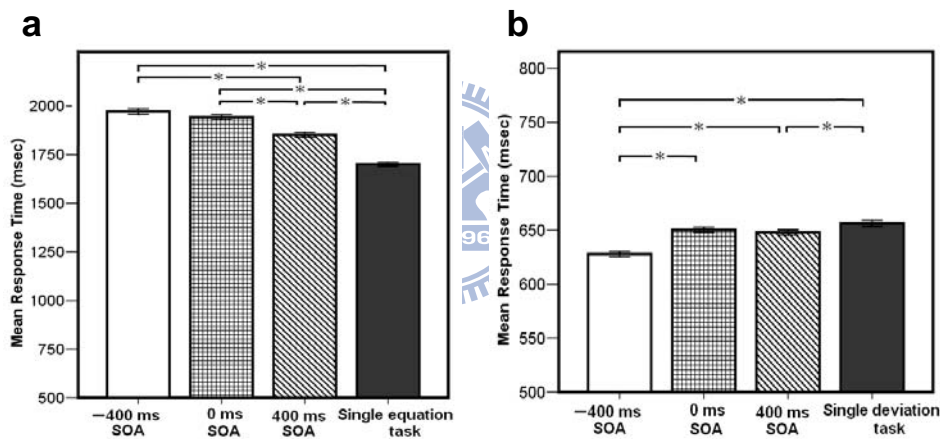


Fig. 4-4: Statistical significance of the dual tasks in each condition was analyzed by repeated measures ANOVA followed by pair wise comparisons. Error bar indicates  $\pm 1 \cdot \text{SE}$ . Panel (a) shows mean response time for responding car deviation. The repeated measures ANOVA test reveals RT of  $-400\text{ms}$  SOA condition was significantly lower than those in other conditions. Panel (b) shows mean response time for answering math questions. The repeated measures ANOVA test results show that RT in the  $-400\text{ms}$  SOA condition was significantly higher than those in other conditions except in the  $0\text{ms}$  SOA condition.

To eliminate the individual differences, normalized mean RTs were computed for every subject in all conditions. Friedman ANOVA statistic test was used to assess the driving performance and interference effects (as shown in Fig. 4-5).

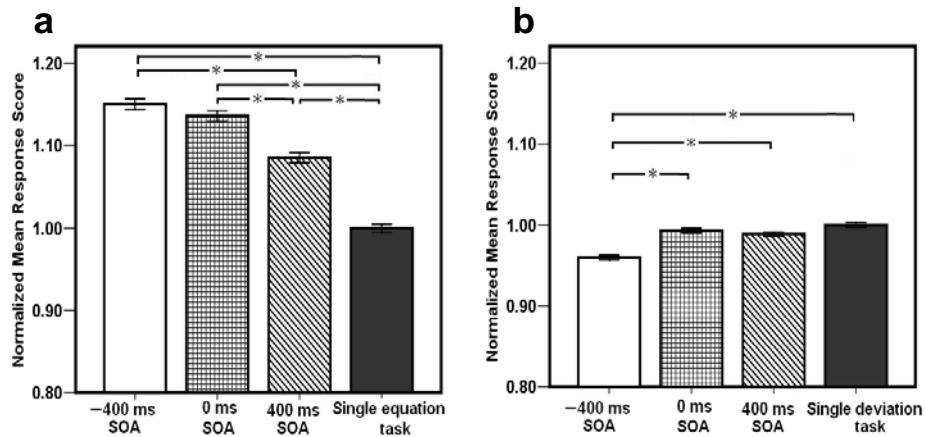


Fig. 4-5: Statistical significance of the dual tasks in each condition was analyzed by Friedman ANOVA followed by pair case comparisons using the Dunnett T3 method. Error bar indicates  $\pm 1 \cdot SE$ . Panel (a) shows normalized mean response score for responding car deviation. The Friedman ANOVA test reveals RT of  $-400\text{ms}$  SOA condition and single deviation task were significantly different. The test also reveals no significant differences existed among  $0\text{ms}$  SOA,  $400\text{ms}$  SOA and single deviation task conditions. Panel (b) shows the normalized mean response score for answering math equations. The Friedman ANOVA test results show that RT in the  $-400\text{ms}$  SOA condition was significantly higher than those in other conditions except in the  $0\text{ms}$  SOA condition.

In Fig. 4-5a, the statistic results of Friedman ANOVA test shows a significant effect in responding the car deviation task ( $p < 0.01$ ). Moreover, the Dunnett T3 test demonstrates that a significant difference existed between the  $-400\text{ms}$  SOA condition and the single task; that is, the  $-400\text{ms}$  SOA condition had a lower normalized mean response score than all other

conditions. In Fig. 4-5b, the experimental results show that answering the math equation task had a significant effect on responding dual tasks. The Friedman ANOVA test indicates a significant effect in answering math equations task ( $p < 0.01$ ). The Dunnett T3 test shows that a significant difference existed between the single-task and three dual-task conditions.

## 4.5 Dual-task Distraction Effects

In the first condition ( $-400\text{ms SOA}$ ) which the math equation task appeared before the driving task 400 ms, the performance was dominated in solving complex arithmetic problems because the subjects needed to use more workload and exploit the limited-capacity resources in solving math equations based on their mental calculation level. In addition, this study also found that the subjects were likely to solve the math equations later than responding the car deviation because the difficulty of responding the car deviation task was easier than that of answering math equation task. So the subjects were likely responding the car deviation based on their subconscious reflection. Hence, the RT of responding the math equation tasks was the slowest under the first condition. Furthermore, according to the RT of the first condition, answering the math equation task did not increase the difficulty of responding driving task. That was also the reason why the perceptual bottleneck in answering the math equation task had no effect on responding the car deviation task. Moreover, when the subjects faced the math equations first and then the car suddenly deviated, they converted to focus on responding the car deviation instantly, and answering the math equations later. In this situation, subjects did not know when the math equations would appear in advance. This scenario was similar to perform the distracting task while driving in real environment such as answering the cell phone call or talking to the passenger. The driver stopped performing the distracting task immediately until finishing the driving task. Therefore, this study found the evidence that the RT of answering the math equation task in the first condition was the slowest.

In the second condition (0ms SOA), both the math equation and the car deviation tasks were appeared simultaneously. According to the response-selection bottleneck for responding simultaneous tasks of driving and math addition, subjects would reflect three possible underlying sequences: driving response was selected first; answering math equations was the first response; or responses were selected in series. Therefore, subjects might use the trade-off strategy to response in the second condition. In this study, however, they decided to stop performing the math equation task due to their more attention to perform the driving task. To interpret why RT increased when performing dual tasks within a short SOA condition, there were several reasons. First, the strategies of manipulations, which were thought to affect response selection or performance, always affected the RT of answering the math equation task. Second, because the appearance order of tasks was unknown, subjects would perform in series rather than in parallel. Third, due to the high difficulty of answering the math equation task, the more cognitive resources were allocated to answering the math equation task. Furthermore, it suggested that 0ms SOA condition required capacity sharing or involved multiple resources. For example, the central execution could coordinate the performance of multiple simultaneous tasks. Several reasons can be used to interpret the reason why RT will be increasing when performing dual tasks within a short SOA condition.

In the third condition (400ms SOA), which the car deviation was appeared before the math equation 400ms, answering math equation task was easier than that in above two conditions but still more difficult than that in single-task condition. The results showed that responding the car deviation task caused the slight distraction effect on answering the math equation task because the duration of temporal overlap in this condition was lower than RT1 which was the duration of temporal overlap in -400ms and 0ms SOA conditions (as shown in Fig. 4-6). On the other hand, subjects would respond the car deviation task first based on their subconscious reflection and then process the math equation task. The results showed that the math equation task did not cause distraction effects to the subjects to respond the car

deviation task.

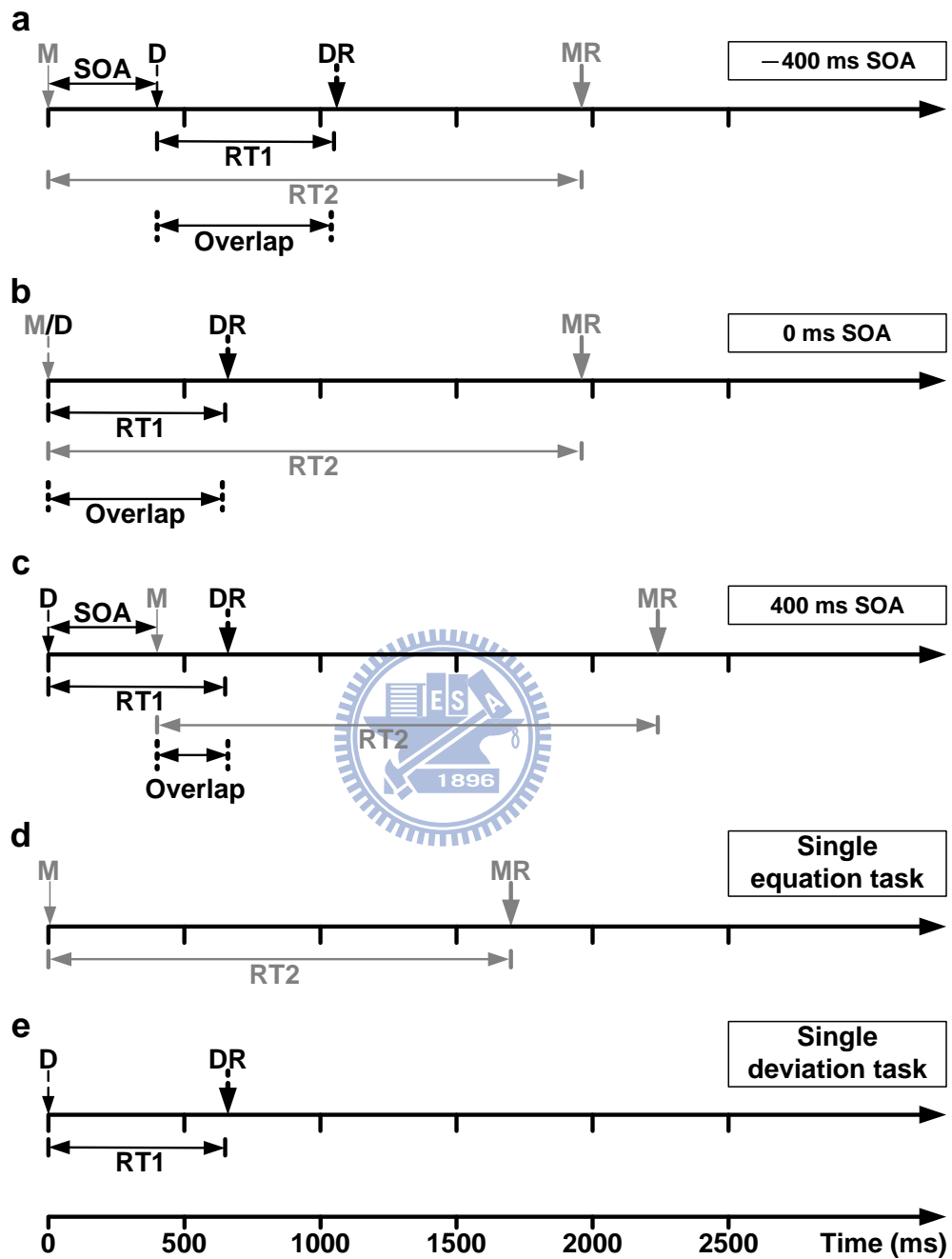


Fig. 4-6: An illustrative time diagram for the SOAs and a single task conditions. (a) In the  $-400\text{ms}$  SOA condition, overlap time of Task 1 and Task 2 is  $RT1$  (high task overlap). (b) In the  $0\text{ms}$  SOA condition, overlap time of Task 1 and Task 2 is also  $RT1$  (high task overlap). (c) In the  $400\text{ms}$  SOA condition, Task 1 and Task 2 overlap time is  $RT1 - \text{SOA}$  (less than  $RT1$ , low task overlap). (d) Only math equation presented. (e)



Only deviation occurred. M: Math equation appeared; MR: Response math equations;  
D: Deviation appeared; DR: Response car deviation.

## 4.6 Brain Dynamics Related to Behavioral Performance

Posner et al. (1989) postulated that two tasks performed simultaneously did not interfere with each other's performance when different brain areas were used for these two tasks. However, this study uses two visual-stimuli tasks that compete within the frontal and motor areas for taking action. From the results, these two visual-stimuli tasks interfere with each other in both behavioral performance (in Fig. 3-1) and brain dynamics (in Fig. 3-11).

In order to compare brain dynamics among different cases (in Fig. 3-11), a statistical analysis was also conducted to assess the significance of the ERSP differences of the independent clusters under different cases. Since the true sample distribution of the cluster ERSP was unknown and the sample size ( $N=14$  as 1 of 15 subjects and  $N=11$  as 4 of 15 subjects were excluded in frontal and left motor clusters, respectively) was small, a nonparametric statistical analysis, a paired-sample Wilcoxon signed-rank test, was employed to assess the statistically significant ERSP differences under different cases. The level of significance was set to  $p < 0.01$ .

In Fig. 3-11c, the significant differences between dual-task cases and case 4 are due to that subjects' reaction to a math question is impaired when they are also facing a car deviation. Lavie et al. (2004) demonstrated that dual-task load increases distraction effects. Because of the distraction effects, the behavioral response time are significantly higher in dual-task cases than that in single-task case. In order to study the comparisons of these dual-task cases, the differences of them are shown in Fig. 3-11b. From the behavioral performance in Fig. 3-1, response time in case 1 and case 2 are the longest which means that the most distraction effects occurred in these two cases. It is also shown in Fig. 3-11b. Especially, distraction

effects in case 1 are slightly higher than those in case 2. Therefore, it is suggested that some kinds of two sequent tasks make the same distraction effects as two simultaneous tasks, or even higher.

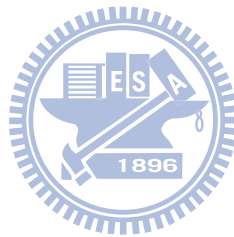
Jong (1995) investigated how performance of two overlapping discrete tasks was organized and controlled. The sequential performance of overlapping tasks can be scheduled in advance and regulated by initially allocating brain resources to one task and subsequently switching to the other task. Thus in case 1, when the math task is presented to the subject, it occupies the brain resources. Then because the driving task appears, the brain resources are immediately switched to the driving task and the math task is temporally dropped. Subsequently, the brain resources are then switched back to the math task. This processing consumes the most brain resources and makes the longest response time for the math question. The response time in case 1 is significantly higher than that in case 3 and case 4. The occurrence of distraction effects is due in large part to the switching of brain resources.

The fact, which no significant differences occur on behavioral performance for the driving tasks between the simultaneous-task case 2 and single-task case 5 (in Fig. 3-1), suggests that the driving task is too simple to require much brain resources. These results are also due to the first priority on the driving task. No differences of behavioral performance, which appear among case 2, case 3 and case 5, also prove this fact. Thus, the subjects always chose to respond to the driving task when the driving task occurs even if they are handling a math task. In case 1, however, the math question is taken as a cue to let the subjects rapidly respond to the driving task to avoid hitting the wall. This situation makes the response time short for the driving task in case 1 due to the subjects under a high perceptual load. Consistently, Lavie et al. (2004) demonstrated that a high perceptual load reduced response time. This also causes case 1 and case 3, which are formed as a symmetrical paradigm, to be much different from each other (in Fig. 3-1).

In Fig. 3-11, the most power suppression occurs in case 5 (in Fig. 3-11f) with only

driving task. Three dual-task cases have the same level of power suppression. The reason why less power suppression occurs on dual-task cases in motor area is suggested that most brain resources are occupied in frontal area to deal with two tasks instead of those in motor area. It is proposed that motor area is not related to distraction effects. This is proved by one more result that the correlation is low between EEG dynamics in motor area and its corresponding response time.

In summary, this study observes several differences between dual-task and single-task cases. We investigate the relationship between brain dynamics associated with dual-task management and the behavioral performance of response modalities. It is suggested that EEG dynamics in the beta band of the frontal area can be indices of distraction effects. In addition, the appearing order of the two tasks with different difficulties is an important factor in dual-task performance.



# Chapter 5

## CNN Implementation

Some studies demonstrated their work in analyzing electroencephalographic (EEG) signals by utilizing Cellular Nonlinear Networks (CNN) which was considered for a multidimensional signal analysis called the feature extraction problem (Tetzlaff et al., 2006). In this chapter, I present a CNN-based Hybrid-order Texture Segregation as Early Vision Processing. In the future, I will like to implement EEG hardware by CNN features and architecture.

### 5.1 Cellular Neural Networks (CNN)

The Cellular Neural Network (CNN), also known as the Cellular Nonlinear Network, first introduced by Chua and Yang (1988), as an able to implement alternative to fully connected neural networks, has evolved into a paradigm for those types of array (Chua and Roska, 1993). The CNN paradigm provides the framework for the computation of an algorithmically programmable array computer on a chip: named the CNN Universal Machine (CNN-UM). Its powerfully computing characteristic enables the realization of complex image processing tasks. However, it is not necessary to construct complex analog-logical circuits, such as the CNN-UM for a special CNN application. Thus, we aim at the property of the proposed algorithm to design a suitable CNN-based circuit.

### 5.2 CNN-based Hybrid-order Texture Segregation

In this chapter, a new boundary detection algorithm is proposed (in Fig. 5-1). This

algorithm combines the first and the second order features for modeling the pre-attentive stage of human visual system.

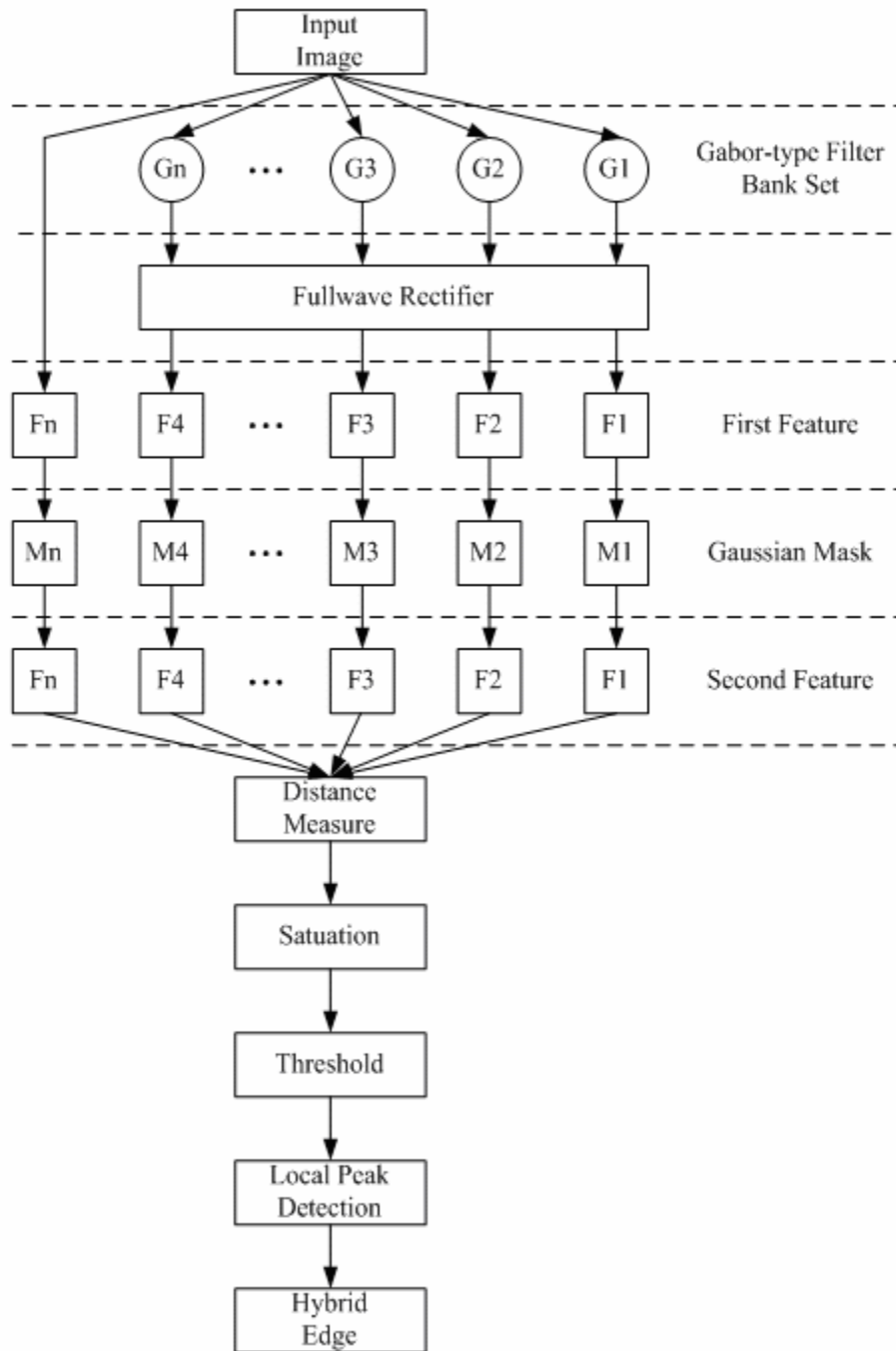



Fig. 5-1: The diagram of proposed algorithm

Fig. 5-1 shows the flow chart of the proposed approach: first, the first order features have been extracted by the Gaussian low-pass filters and the second order features have been

extracted by the Gabor filters, respectively. Assume that each pixel of the output is defined by a  $N+1$  dimensional vector. After the first order features extraction, the vector contains  $N$  Gabor filters and 1 Gaussian filter. Next, we measure the difference of each pixel with its neighbor. Since the pixels, which belong to the same region have similar features, the level of difference among those pixels should be smaller than the difference to pixels existing in other regions of the image. Third, we keep these pixels with values larger than a specific threshold, and set the others to zero. We would get coarse boundaries which are look like Bell-shaped distribution. Consequently, we may go to thin these boundaries by a local peak detection. Finally, we can obtain boundaries similar to human visual system. Followed sections are going to introduce each block of the proposed algorithm.

### 5.2.1 Functions of Blocks



**First order Feature Extraction:** As we have introduced in the previous section, the ganglion is accomplished by the so-called “center-surround” organization of the receptive field, in which it’s excitatory and inhibitory subfields are organized into circularly symmetric regions. This fact implies the receptive field of the ganglion is similar to the *Difference of two Gaussians (DoG)*. Subsequently we describe how the DoG function detects boundaries: first, two Gaussian filters with different values of  $\sigma$  are applied in parallel to the images. Afterwards the difference of the two smoothed instances is computed. It can be shown that the DoG operator approximates the LoG one which has been widely used in boundary detection.

**Second order Feature Extraction:** The receptive fields of V1 cells are orientation selective, and it can be modeled by the Gabor function (Chen, 1999; Hawkins, 1969). The Gabor function is an adaptive band-pass filtering method which constructs a complete but non-orthogonal basis set. On the other hand, the Gabor function consists of a Gaussian function which is modulated by a sinusoidal function.

**Gabor Filtering Bank Set:** Besides the orientation selectivity, the Gabor filters are also frequency selective. With these two properties, Daugman extended the original Gabor filter to a two-dimensional (2D) representation (Daugman et al., 1985). There are many researches which focus on the Gabor filter bank. Jain and Farrokhnia (1981) suggested a bank of Gabor filters, i.e., Gaussian shaped band-pass filters, with dyadic coverage of the radial spatial frequency range and multiple orientations. Fig. 5-2 shows an example of the Gabor filtering bank set. Since the goal of this chapter is designing an algorithm which can be implemented on the CNN-UM, the structure could not be complex-valued. In this chapter, we use four Gabor filters for extracting the second order features in the experiments. All of these Gabor filters have the same Gaussian shape in the frequency domain and scatter uniformly in four orientations.

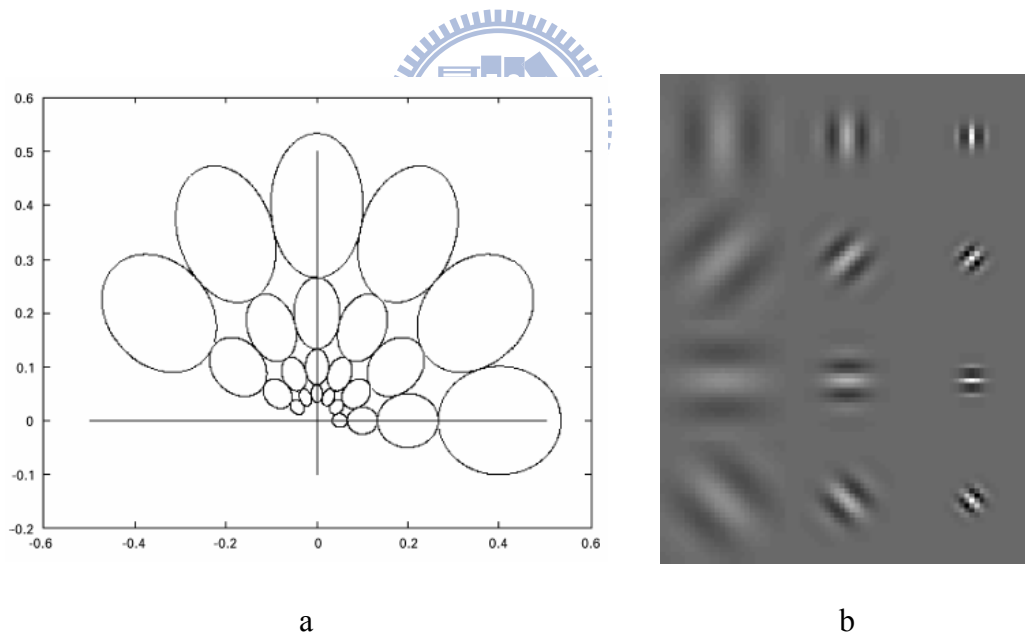


Fig. 5-2: An example of Gabor filter dictionary. (a) represents the Gabor-type filter bank set, and (b) is the Feature space of Gabor filter dictionary.

**Full-wave Rectification:** Just like the other filter-rectify-filter model, the rectifying operation is taken after the operation of the Gabor filters. It has been generally acknowledged

that V1 cells have a property which looks like the half wave rectification. The intervening rectification ensures that the fine-grain positive and negative portions of the carrier will not disable another when the smoothing operation is performed.

**Gaussian Post Filtering:** After the cells were stimulated by a specific signal, for example, a bar with specific orientations, the output of the V1 cells responding to same direction will aggregate together. The region of cells which contain the same properties will respond stronger than the other regions. It is consistent with the “localization” properties of the textures. This effect can be simulated by a Gaussian post filters. It looks like the averaging with different weighting which is inverse proportional to the distance from the center of the post filter.

**Difference Measure:** The features which have been extracted by Gaussian post filtering can be described by an N-dimensional vector. Each feature vector can be regard as a point in N-dimensional space. According to Chen (1994), the difference is represented by the distance in N-dimensional space (Chen, 1994). There is an important property of the textures. That is the pixels which are aggregated together usually contain similar features. Based on this property, some algorithms use gradient for extracting the features (Tan, 1995). In this chapter, we only calculate the difference between features of each pixel to pixels right behind and below to it.

**Saturation:** In proposed algorithm, when there are more than two kinds of textures in the test patterns, there will be more than one boundary. Because these boundaries usually do not have similar intensity, choosing threshold becomes an important problem. For the sake of finding the threshold, we use the mean of the difference of the total pixels as the threshold. Usually, some boundaries with relative lower magnitude are eliminated. This is because of follows: first, a relative huge region be considered for measuring the local feature. Next, the scale of difference between different patterns varies enormously. Obvious boundaries and cause relatively larger difference and raise the mean of difference. The boundaries which are



not so obvious causing relative lower difference will be eliminated. For attacking this problem, a natural-log transform can be used for simulating the saturation effect. It can suppress stronger responses which may affect the threshold too much. Meanwhile, it still keeps the location of maximum difference where we assume boundaries lying. The strength of the responses reflects the level of differences between two local regions, but it may be not so linearly consistent to our perceptual feeling. According to some biological theories, in the human vision system, the dynamic range of response is limited, and the range of response is not linearly proportional to stimulate (Treisman, 1986). Natural log transform is an ordinary and important operation and it stretch the range of lower responses where we need to judge whether there are boundaries or not.

**Local Maximum Detection:** The coarse boundaries detected after taking threshold generates a range where the boundaries are probably located on. Thus, local maximum detection is used to detect the best assumption of the location of the boundaries. It assumes that the difference among different patterns should be maximal at their boundary. For the implement of the Local Maximum Detection in CNN, the template can be defined as follows:

$$A = \begin{bmatrix} 0 & 0 & 0 \\ 0 & 3 & 0 \\ 0 & 0 & 0 \end{bmatrix}, B = \begin{bmatrix} b & b & b \\ b & 0 & b \\ b & b & b \end{bmatrix}, z = 3.5, \quad (1)$$

where

$$b = \begin{cases} 0.5 & \text{if } v_{u_{ij}} - v_{u_{kl}} \geq 0 \\ 0 & \text{otherwise} \end{cases} \quad (2)$$

Eq.(1) and Eq.(2) perform what we need.

## 5.3 Experimental Results

We applied our algorithm to the images which consist of a number of different test patterns. Most of those test patterns are synthesized by textures from Brodatz album, 1966 and it also has become a standard for evaluating texture algorithms. Each texture pattern we used here are 640\*640 pixel 8-bit gray-scale images respectively. In the experiments, the proposed algorithm has been simulated on CNN-UM.

The proposed algorithm has been implemented on ACE4K Chip. Because of the limitation of current technology, the size of cell array has been limited. That becomes to the major problem in the implementation of proposed algorithm on CNN-UM. For example, the chip we used for implementing proposed algorithm contains cell array 64 by 64. It is too small to analyze the texture. For the sake of higher resolution for obtaining better performance, some necessary operations have been performed before proposed approach: first, each input image has been divided into several sub-images. Next, we process each sub-image respectively with same parameters. Fig. 5-3 shows how we divide the input images. Note that there are overlapped areas between sub-images because we have to avoid the boundary effects of the cell array.

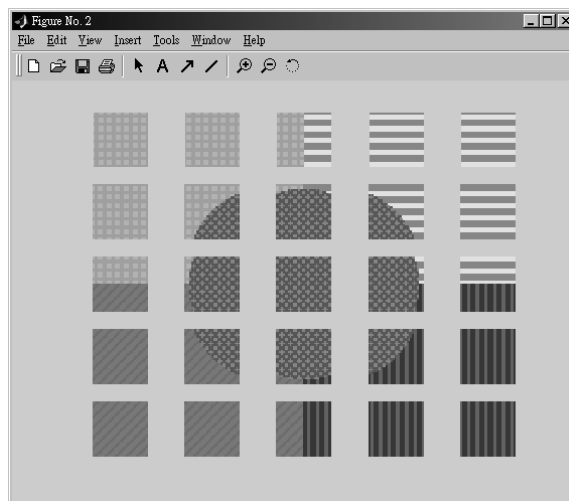


Fig. 5-3: The example of dividing of the input images.

Another issue in the implementation of proposed algorithm on CNN-UM is that we are not able to implement non-linear templates on the chip. Thus, several proposed operation is not able to be implemented directly. For those operations, we choose another operation which is able to be implemented on the chip and the result is similar to what we expected. Even more, we have to disable some operations in proposed algorithm and take the trade-off. For example, Local Maximum Detection operation contains nonlinear template and thus, it can not be implemented on ACK4K Chip. Hence, we choose BLACK\_AND\_WHITE\_SKELETONIZATION to replace it. Fig. 5-4 shows the results of implementation of proposed algorithm on ACE4K Chip.

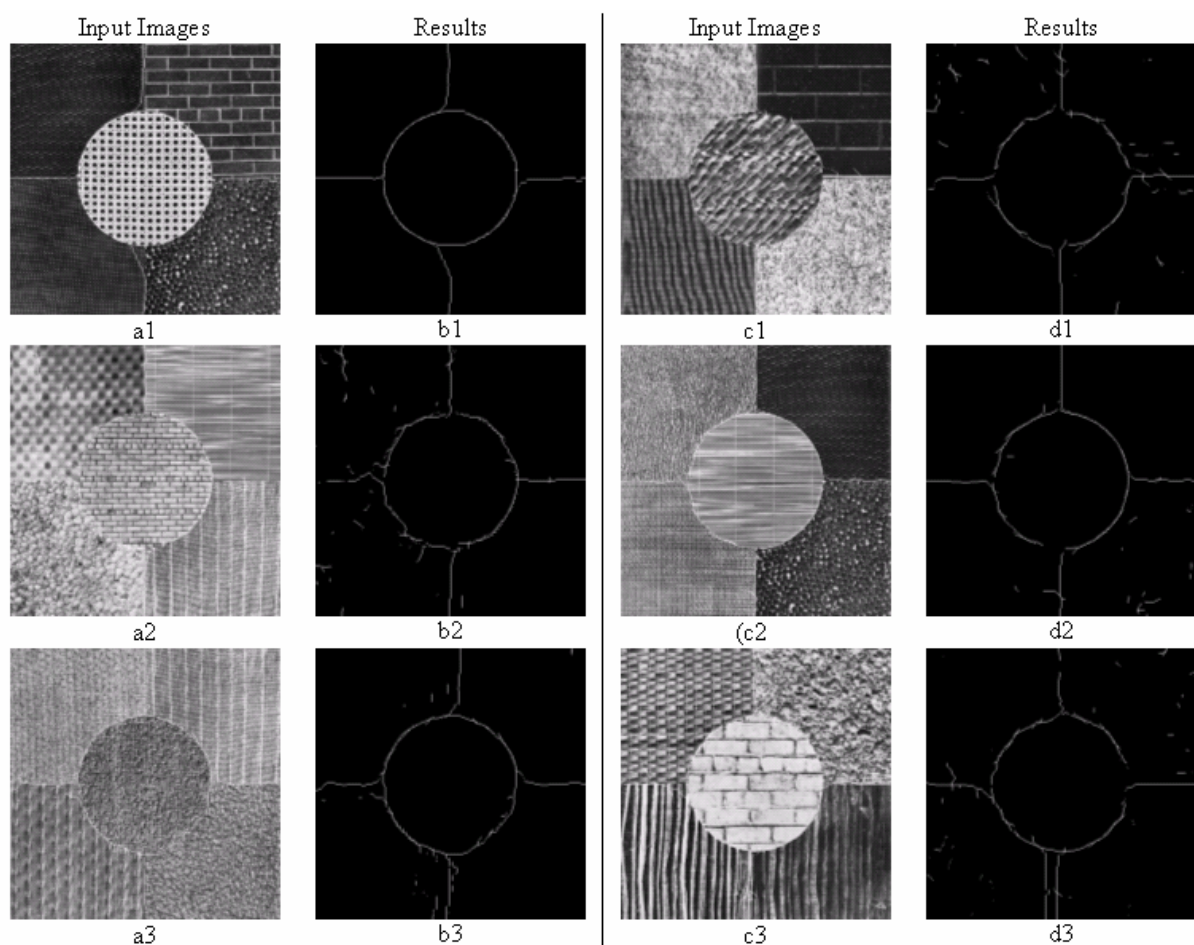


Fig. 5-4: The simulation results of proposed algorithm.

## 5.4 Discussion

In this section, we discuss some properties of the proposed approach. The way we estimate the error is as follows:

Only the case that synthesizes two texture patterns in Brodatz texture is considered. In the algorithm, every boundary is independently. It is hard to judge the accuracy if we consider multi-boundaries simultaneously. Especially when some boundaries are detected and the others are not.

The distance between the answer and the result detected by the algorithm is measured in the condition of boundary which is detectable. We define the error by dividing measured distance into the number of total pixels.

Fig. 5-5 is a histogram of error estimation in our experiment, and the results with error less than 5% is account for 85% for test images. The average of the error is less than 5%. The smallest error is 0.76%. Note that the images with bigger estimated errors are reasonable. In these examples, the boundaries between different textures (middle line) exist, but they are weaker than local boundaries caused by non-uniform regions. For the sake of simplicity, only the largest peaks are kept during error estimation, so the boundaries in the middle are not kept in the results. Although in these examples, the outputs are consistent to human visual perception. Their errors are quite big. We have found that it is hard to define a generally “correct answer” for all test images in human vision system, and the method we measure the error is probably not suited for those kind of test images. For this reason, the measurement is not necessary for the input images synthesized by the rest 42 textures in Brodatz textures.

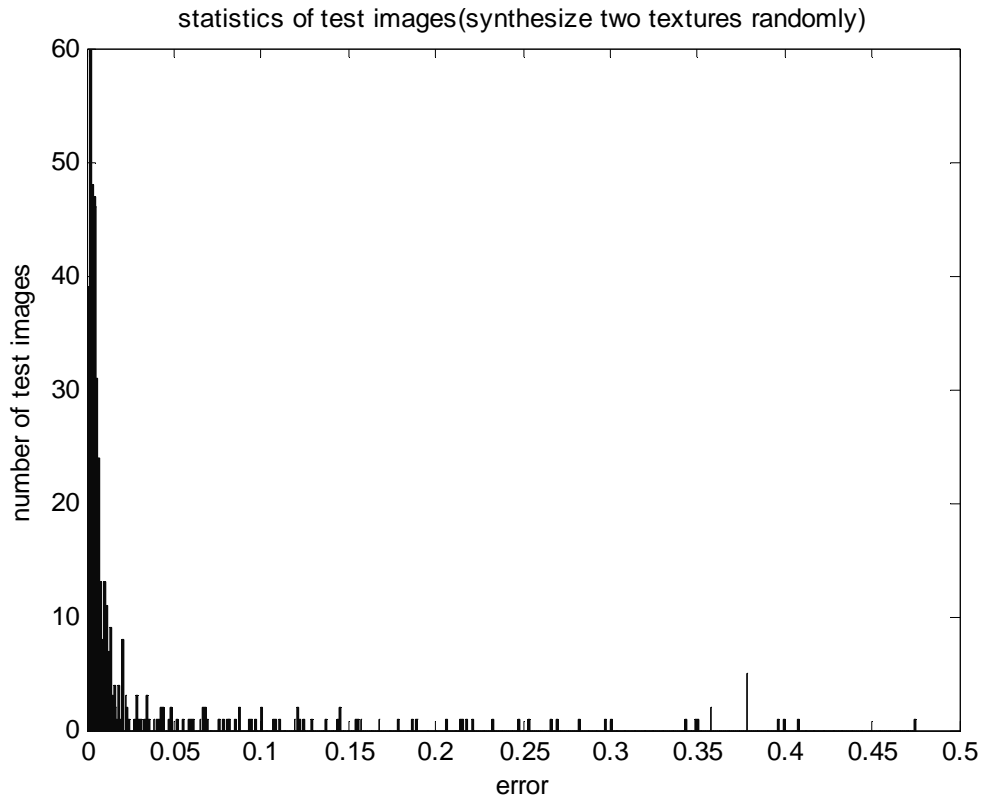
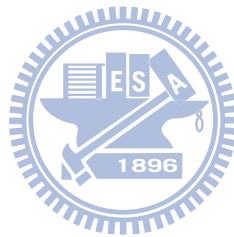


Fig. 5-5: Histogram of error estimation

In summary, a simple framework for hybrid-order boundary detection is proposed. It mimics the mechanism of the early stage of the human vision, and experimental results are generally consistent to the human visual sensation. After post processing, the detected boundaries also have adequate accuracy for the other image processing applications such as stereo, and pattern recognition. By implementing the proposed algorithm on the Cellular Neural Networks (CNN), the computational time will greatly decrease. The real-time processing capability is critical in some applications, such as the object tracking. As same as the other algorithms for textures analysis which is also based on the Gabor filters, there are too many parameters need to be determined. Determining the parameters will much more complex when the synthesized texture patterns increased. For the sake of keeping the structure simple and combining the hybrid-order features easily without the clustering methods, we use same resolution for all of the Gabor filters in the approach. In this approach,

we only consider the first and the second order features. According to some research results, there are still some higher-order features that can be utilized. For example, color is one of them. We do believe proposed approach can be extended to color textures by integrating color information.



# Chapter 6

## Conclusion

This study investigates behavioral and EEG responses under multiple cases and multiple distraction levels. Firstly, the response time for mathematical problem solving in dual-task condition is significantly higher than that in single-task condition. Therefore, distraction effects occur while processing two tasks during driving. Comparing to the mathematical problems, however, the response time for driving tasks under multiple cases is almost the same without differences. This is due to the order of task appearance and the relative difficulty of the two tasks, which suggesting these factors are important considerations in dual-task performance. Secondly, theta power increases in the frontal area are higher with higher response time. The phasic changes around the theta band in the case, in which the mathematic task is presented before the deviation task, show the strongest increase as the same as that in the simultaneous-task case. This is because subjects already process a task in the brain and need more brain resources to manage the second task presented after the first task. In conclusions, this study suggests that the power increases of the 4~7.8 Hz frequency band in the frontal area is related to driver distraction and represents the strength of distraction in real-life driving.

For the future work, we will still work hard on EEG research for keeping safety during driving. Can we detect the mistake happened by watching the EEG power before it happens? How long can we detect it before it happens?

Based on the good properties of CNN, on the other hand, we are working on implementing the EEG analysis on CNN which was considered for a multidimensional signal analysis. In the future, I will like to implement EEG hardware by CNN features and architecture.

# References

Amado S, Ulupinar P: The effects of conversation on attention and peripheral detection: is talking with a passenger and talking on the cell phone different? *Transportation Research* 2005, 8, 383-395.

Baldwin CL, Coyne JT: Mental workload as a function of traffic density: Comparison of physiological, behavioral, and subjective indices. *Proceedings of the Second International Driving Symposium on Human Factors* 2003.

Brodatz P: *Textures: a Photographic Album for Artists and Designers*. New York: Dover Publications, 1966.

Burgess PW: Strategy application disorder: the role of the frontal lobes in human multitasking. *Psychophysiology* 2000, 63, 279-288.

Chen I: *Texture Perception: A Linear System Approach*. University of California, Berkeley, 1994.

Chen I: Visual and visuomotor processes. *Vision and cognition*. Taipei: Yuan-Liou, 1999, pp. 128-158.

Chua LO, Roska T: The CNN Paradigm. *IEEE Trans. Circuits Syst. - II*, vol. 40, pp. 147-156, 1993.

Chua LO, Yang L: Cellular neural networks: theory. *IEEE Transactions on Circuits and Systems*, vol. 35, pp. 1257-1272, 1988.

Corbetta M, Miezin FM, Dobmeyer S, Shulman GL, Petersen SE: Selective and divided attention during visual discriminations of shape, color, and speed: functional anatomy by



positron emission tomography. *J Neuroscience* 1991, 11, 2383-2402.

Crundall D, Loon EV, Underwood G: Attraction and distraction of attention with roadside advertisements. *Accident Analysis & Prevention* 2006, 38, 671-677.

Daugman J: Uncertainty Relation for Resolution in Space, Spatial Frequency, and Orientation Optimised by Two-Dimensional Visual Cortical Filters. *Journal of the Optical Society of America*, vol. 2, pp. 1160-1169, 1985.

Deiber MP, Missonnier P, Bertrand O, Gold G, Fazio-Costa L, Ibañez V, Giannakopoulos P: Distinction between perceptual and attentional processing in working memory tasks: a study of phase-locked and induced oscillatory brain dynamics. *Journal of Cognitive Neuroscience* 2007, 19, 158-172.

Dukic T, Hanson L, Falkmer T: Effect of drivers' age and push button locations on visual time off road, steering wheel deviation and safety perception. *Ergonomics* 2006, 49, 78-92.

Eoh HJ, Chung MK, Kim SH: Electroencephalographic study of drowsiness in simulated driving with sleep deprivation. *International Journal of Industrial Ergonomics* 2005, 35, 307-320.

Fernández T, Harmony T, Rodríguez M, Bernal J, Silva J, Reyes A, Marosi E: EEG activation patterns during the performance of tasks involving different components of mental calculation. *Electroencephalogr Clin Neurophysiol* 1995, 94, 175-182.

Geary DC, Wiley, JG: Cognitive addition: strategy choice and speed-of-processing differences in young and elderly adults. *Psychology and Aging* 1991, 6, 474-483.

Hahn RW, Tetlock PC, Burnett JK: Should you be allowed to use your cellular phone while driving? *Regulation* 2000, 23, 46-55.

Hancock PA, Lesch M, Simmons L: The distraction effects of phone use during a crucial

driving maneuver. *Accident Analysis & Prevention* 2003, 35, 501-541.

Hawkins JK: *Picture Processing and Psychopictories. Textural Properties for Pattern Recognition*, B. Lipkin and A. Rosenfeld, Eds. New York: Academic Press, 1969.

Hayhoe M, Shrivastava A, Mruczek R, Pelz JB: Visual memory and motor planning in a natural task. *Journal of Vision* 2003, 6, 49-63.

Horberry T, Anderson J, Regan MA, Triggs TJ, Brown J: Driver distraction: the effects of concurrent in-vehicle tasks, road environment complexity and age on driving performance. *Accident Analysis & Prevention* 2006, 38, 185-191.

Jensen SM, Barabasz A, Barabasz M, Warner D: EEG P300 event-related markers of hypnosis. *Clinical Hypnosis* 2001, 44, 127-39.

Jong RD: The role of preparation in overlapping-task performance. *Quarterly Journal of Experimental Psychology* 1995, 48, 2-25.

Jung TP, Makeig S, Humphries C, Lee TW, McKeown MJ, Iragul V, Sejnowski TJ: Removing electroencephalographic artifacts by blind source separation. *Psychophysiology* 2000, 37, 163-78.

Kandel E, Schwartz J, Jessell T: *Principles of Neural Science*, 3rd edition.

Kemeny A, Panerai F: Evaluating perception in driving simulation experiments. *TRENDS in Cognitive Sciences* 2003, 7, 31-37.

Koechlin E, Basso G, Pietrini P, Panzer S, Grafman J: The role of the anterior prefrontal cortex in human cognition. *Nature* 1999, 399, 148 -151.

Kuhlman WN: EEG feedback training: enhancement of somatosensory cortical Activity. *Electroencephalogr Clin Neurophysiol* 1978, 45, 290-294.

Kuhlman WN: Functional topography of the human Mu rhythm. *Electroencephalogr Clin Neurophysiol* 1978, 44, 83-93.

Lavie N, Hirst A, Fockert JW, Viding E: Load Theory of Selective Attention and Cognitive Control. *Journal of Experimental Psychology* 2004, 9, 339-354.

Lee JD, Caven B, Haake S, Brown TL: Speech-based interaction with in-vehicle computers: the effect of speech-based e-mail on drivers' attention to the roadway. *Human Factors* 2001, 43, 631-640.

Lee TW, Girolami M, Sejnowski TJ: Independent component analysis using an extended infomax algorithm for mixed sub-Gaussian and super-Gaussian sources. *Neural Computation* 1999, 11, 606-633.

Levy J, Pashler, H: Is dual-task slowing instruction dependent? *Journal of Experimental Psychology: Human Perception and Performance* 2001, 27, 862-869.

Lin CT, Chen YC, Huang TY, Chiu TT, Ko LW, Liang SF, Hsieh HY, Hsu SH, Duann JR: Development of Wireless Brain Computer Interface With Embedded Multitask Scheduling and its Application on Real-Time Driver's Drowsiness Detection and Warning. *IEEE Trans BME* 2008, 55, 1582-1591,

Lin CT, Huang KC, Chao CF, Chen JA, Chiu TW, Ko LW, Jung TP: Tonic and phasic EEG and behavioral changes induced by arousing feedback. *NeuroImage* 2010, 52, 633-642.

Lin CT, Wu RC, Jung TP, Liang SF, Huang TY: Estimating Driving Performance Based on EEG Spectrum Analysis. *EURASIP Journal on Applied Signal Processing* 2005, 19, 3165-3174.

Lin CT, Wu RC, Liang SF, Huang TY, Chao WH, Chen YJ, Jung TP: EEG-based Drowsiness estimation for safety driving using independent component analysis. *IEEE Transactions on*

Circuit and System 2005, 52, 2726-2738.

Makeig S, Bell AJ, Jung TP, Sejnowski T: Independent component analysis of electroencephalographic data. *Advance in Neural Information Processing System* 1995, 8, 145-151.

Makeig S, Delorme A, Westerfield M, Jung TP, Townsend J, Courchense E, Sejnowski TJ: Electroencephalographic brain dynamics following visual targets requiring manual responses. *PLOS Biology*, 2004, 2, 0747.

Makeig S, Inlow M: Lapses in Alertness: Coherence of Fluctuations in Performance and EEG Spectrum. *Electroencephalography. Clin. Neurophysiol* 1993, 86, 23-35.

Makeig S, Westerfield M, Jung TP, Enghoff S, Townsend J, Courchesne E, Sejnowski TJ: Dynamic brain sources of visual evoked responses. *Science* 2002, 295, 690-694.

Makeig S: Auditory event-related dynamics of the EEG spectrum and effects of exposure to tones. *Electroencephalography and Clinical Neurophysiology* 1993, 86, 283-293.

Missonnier P, Deiber MP, Gold G, Millet P, Pun MG., Fazio-Costa L, Giannakopoulos P, Ibáñez V: Frontal theta event-related synchronization: comparison of directed attention and working memory load effects. *Journal of Neural Transmission* 2006, 10, 1477-1486.

Onton J, Delorme A, Makeig S: Frontal Midline theta dynamics during working memory. *Neuroimage* 2005, 27, 341-356.

Oostenveld R, Oostendorp TF: Validating the boundary element method for forward and inverse EEG computations in the presence of a hole in the skull. *Hum. Brain Mapp* 2002, 17, 179-192.

Patten CJD., Kircher A, Östlund J, Nilsson L: Using mobile telephones: cognitive workload and attention resource allocation. *Accident Analysis & Prevention* 2004, 36, 341-350.

Posner MI, Sandson J, Dhawan M, Shulman GL: Is word recognition automatic? A cognitive-anatomical approach. *Journal of Cognitive Neuroscience* 1989, 1, 50-60.

Rakauskas ME, Ward NJ, Bernat EM, Cadwallader M, Patrick CJ, Waard D: Psychophysiological measures of driver distraction and workload while intoxicated. *International Symposium on Human Factors in Driver Assessment, Training, and Vehicle Design* 2005, 6, 27-30.

Sarnthein J, Petsche H, Rappelsberger P, Shaw GL, Stein AV: Synchronization between prefrontal and posterior association cortex during human working memory. *Proc Natl Acad Sci U.S.A.* 1998, 95, 7092-7096.

Schoppenhorst M, Brauer F, Freund G, Kubichi St: The significance of coherence estimates in determining central alpha and mu activities. *Electroencephalogr Clin Neurophysiol* 1980, 48, 25-33.

Stelzel C, Schumacher EH, Schubert T, D'Esposito M: The neural effect of stimulus-response modality compatibility on dual-task performance: an fMRI study. *Psychological Research* 2005, 70, 514-525.

Strayer DL, Drews FA, Johnston WA: Cell phone-induced failures of visual attention during simulated driving. *Journal of Experimental Psychology* 2003, 9, 23-32.

Szameitat AJ, Lepsien J, Cramon DY, Sterr A, Schubert T: Task-order coordination in dual-task performance and the lateral prefrontal cortex: an event related fMRI study. *Psychological Research* 2006, 2, 1-12.

Tan TN: Texture edge detection by modelling visual cortical channels. *Pattern Recognition*, vol. 28, pp. 1283-1298, 1995.

Tetzlaff R, Niederhofer C, Fischer P: Automated detection of a pre seizure state: Non-linear

EEG analysis in epilepsy by Cellular Nonlinear Networks and Volterra systems. International Journal of Circuit Theory and Applications 2006, 34, 89-108.

Thomas AR: Driver Distraction: A Review of the Current State-of-Knowledge. National Highway Traffic Safety Administration Vehicle Research and Test Center 2008, DOT F,1700.7 (8-72).

Tijerina L, Johnston S, Parmer E, Winterbottom MD, Goodman M: Driver distraction with route guidance systems. National Highway Traffic Safety Administration 2000, Technical Report No. DOT HS 809-069.

Treisman A: Features and objects in visual processing. Scientific American, vol. 254, pp. 114-125, 1986.

